Inorg. Chem. **2009**, *48*, 68−81

Ruthenium(II) Complexes Incorporating 2-(2′-Pyridyl)pyrimidine-4-carboxylic Acid

Nickita Nickita,[†] Gilles Gasser,[†] Pauline Pearson,[†] Matthew J. Belousoff,[†] Lai Y. Goh,[‡] Alan M. Bond,[†] Glen B. Deacon,[†] and Leone Spiccia*,[†]

School of Chemistry, Monash University, VIC 3800, Australia, and Department of Chemistry, National University of Singapore, Singapore

Received May 28, 2008

A new bidentate ligand bearing a single carboxylate functionality, 2-(2′-pyridyl)pyrimidine-4-carboxylic acid (cppH), has been prepared and applied in the synthesis of a series of ruthenium(II) complexes. Reaction of this new ligand with $Ru^{II}(bpy)_2Cl_2$ led to the unexpected oxidation of the starting material to give $[Ru^{III}(bpy)_2Cl_2]Cl \cdot H_2O$ and a low yield of $[Ru^{II}(bpy)_2(cppH)](PF_6)_2 \cdot H_2O$ (**1**) on addition of an aqueous KPF_6 solution (bpy = 2,2′-bipyridine and cpp = 4-carboxylate-2′-pyridyl-2-pyrimidine). An X-ray crystal structure determination on crystals of **1a**, $[Ru^{II}(bpy)_2(cpp)](PF_6)$, obtained from slow evaporation of an aqueous solution of **1** revealed that the nitrogen para to the carboxylate group in the cpp^- ligand coordinates to the ruthenium(II) center rather than that ortho to this group. The same complex was prepared via decarbonylation of $[Ru^{II}(cppH)(CO)_2Cl_2] \cdot H_2O$ in the presence of bpy and an excess of trimethylamine-N-oxide (Me_3NO), as the decarbonylation agent. The coordination of cppH in the precursor is the same as in the final product. The related complex $[Ru^{II}(phen)_2(cppH)](PF_6)_2 \cdot 2H_2O$ (**2**) (phen = 1,10-phenanthroline) was similarly synthesized. $[Ru^{II}(bpy)(dppz)(cppH)](PF_6)_2 \cdot CH_3CN$ (**3**) (dppz = dipyrido[3,2,-a;2′,3-c]phenazine) was also prepared by photochemical decarbonylation of $[Ru^{II}(bpy)(CO)_2Cl_2]$ giving $[Ru^{II}(bpy)(CO)Cl_2]_2$ followed by bridge splitting with dppz to generate $[Ru^{II}(bpy)(dppz)(CO)Cl](PF_6) \cdot H_2O$. This intermediate was then reacted with cppH to produce **3**, as a mixture of geometric isomers. In contrast to **1**, X-ray crystallography on the major product isolated from this mixture, $[Ru^{II}(bpy)(dppz)(cpp)](NO_3) \cdot 10H_2O$, $\mathbf{3^{N3}}$ indicated that the nitrogen adjacent to the carboxylate was coordinated to ruthenium(II). Full characterization of these complexes has been undertaken including the measurement of UV−visible and emission spectra. Electrochemical and spectroelectrochemical studies in acetonitrile show that these complexes undergo reversible oxidation from Ru^{II} to Ru^{III} at potentials of 983 ± 3 mV, 1004 ± 5 mV, and 1023 ± 3 mV versus $Fc^{0/+}$ (Fc = Ferrocene) for **1**, **2**, and $\mathbf{3^{N3}}$, respectively.

Introduction

Ruthenium(II) compounds containing polypyridyl ligands exhibit a combination of properties, for example, high chemical stability, long-lived excited-state lifetimes, and reversible electrochemical behavior, that make them ideal candidates for a plethora of applications.[1−14] The ability of these types of complexes to be attached to substrates via ester or amide linkages, coupled with their redox and emissive properties, has provided a major impetus to their use in the biosensing area.[15−18] For example, Metzler-Notle et al. have attached $[Ru^{II}(bpy)_2(Mebpy\text{-}COOH)]^{2+}$ (Mebpy-

* To whom correspondence should be addressed. E-mail: leone.spiccia@sci.monash.edu.au. Fax: +61 3 9905 4597. Phone: +61 3 9905 4526.
† Monash University.
‡ National University of Singapore.

(1) O'Reagen, B.; Gratzel, M. *Nature* **1991**, *335*, 737–740.
(2) Gratzel, M. *Coord. Chem. Rev.* **1991**, *111*, 167–174; and references therein.
(3) Balzani, V.; Bergamini, G.; Marchioni, F.; Ceroni, P. *Coord. Chem. Rev.* **2006**, *250*, 1254–1266; and references therein.
(4) Balzani, V.; Juris, A.; Venturi, M. *Coord. Chem. Rev.* **1996**, *96*, 759–833; and references therein.
(5) Marin, V.; Holder, E.; Hoogenboom, R.; Schubert, U. S. *Chem. Soc. Rev.* **2007**, *36*, 618–635.
(6) Vos, J. G.; Kelly, J. M. *Dalton Trans.* **2006**, 4869–4883.
(7) Elias, B.; Kirsch-De Mesmaeker, A. *Coord. Chem. Rev.* **2006**, *250*, 1627–1641.
(8) Gorman, B. A.; Francis, P. S.; Barnett, N. W. *Analyst* **2006**, *131*, 616–639.
(9) Chatterjee, D.; Mitra, A.; De, D. S. *Platinum Met. Rev.* **2006**, *50*, 2–12.
(10) Gonzalez-Vilchez, F.; Vilaplana, R. *Met. Compd. Cancer Ther.* **2005**, 321–354.
(11) Thorp, H. H. *Electrocatalytic DNA oxidation Top. Curr. Chem.* **2004**, *237*, 159–181.

10.1021/ic800972x CCC: $40.75
Published on Web 12/03/2008

Scheme 1. Reagents and Conditions[a]

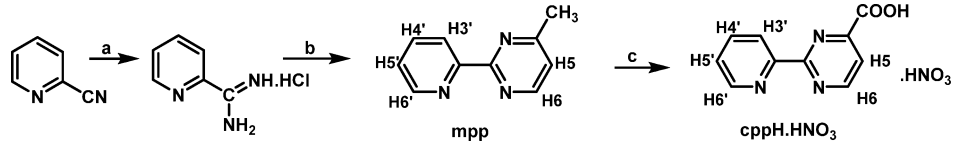

[a] (a) NaOMe, NH_4Cl, MeOH, 22 h. (b) NaOEt, acetylacetaldehyde dimethyl acetal, reflux for 4 h and then stir overnight. (c) conc. HNO_3/HCl (1:1 v/v, reflux, 7h). Labels for proton assignments are included for mpp and cppH·HNO_3.

COOH = 4′-methyl-2,2′-bipyridine-4-carboxylic acid) to Peptide Nucleic Acids (PNAs) to obtain a change in fluorescent and/or electrochemical response on binding to a specific complementary oligonucleotide.[15,19] In this, and other applications such as photosensitization and molecular probing areas,[2,20] the ability to control the spectroscopic and electrochemical properties of Ru^{II} complexes through ligand modification is crucial in the generation of efficient devices. As a consequence, the availability of appropriate synthetic methodology that allows efficient assembly of different chelating polyimine ligands around a Ru^{II} center is vital. Although a number of preparative routes to bis/tris-(diimine)ruthenium(II) complexes have been described,[21] our group has found the synthesis of these metal complexes via a pathway that involves photochemical decarbonylation of $[RuL(CO)_2Cl_2]$ to form $[RuL(CO)Cl_2]_2$ followed by halide bridge splitting with L′ to give $[Ru(L)(L')(CO)Cl]^+$ and subsequent chemical decarbonylation in the presence of either L′ or L″ (L, L′, and L″ = dissimilar diimine ligands) to be a facile and efficient route to $[Ru(L)(L')_2]^{2+}$ and $[Ru(L)(L')(L'')]^{2+}$ complexes.[21−25] Using this approach, a family of ruthenium(II) complexes bearing Mebpy-COOH were synthesized for the first time, and their redox and electronic properties were studied.[26]

Given that the preparation and purification of Mebpy-COOH can prove problematic, alternative mono-functionalized polyimine monocarboxylates capable of incorporation into ruthenium(II) photoactive chromophores, as well as attachment to molecules capable of targeting particular biomolecules, are highly desirable, as this will broaden the range of ruthenium(II) complexes available for biosensing applications. With this in mind, we have developed a new bidentate ligand bearing a single carboxylate functionality, 2-(2′-pyridyl)pyrimidine-4-carboxylic acid (cppH), for incorporation into ruthenium(II) complexes (see Scheme 1). This research extends the work of Rillema and co-workers who reported complexes of the type $[Ru^{II}(bpy)_{3-x}(pypm)_x]^{2+}$, where pypm = 2-(2′-pyridyl)pyrimidine and x = 1, 2, or 3.[27−29] These complexes were found to undergo protonation at the non-coordinated nitrogen of the pyrimidine ring in the ground and excited states and in the one-electron reduced forms.[27−29] To couple these complexes to biomolecule targeting agents, we have introduced a carboxylate functional group into the 2-(2′-pyridyl)pyrimidine ligand. Applying our established methodology,[21,22,24] we have prepared a series of ruthenium(II) complexes incorporating the new asymmetric diimine ligand, $[Ru^{II}(bpy)_2(cppH)](PF_6)_2$ (**1**), $[Ru^{II}(phen)_2(cppH)](PF_6)_2\cdot 2H_2O$ (**2**), $[Ru(bpy)(cpp)(dppz)](PF_6)\cdot H_2O$ (**3**^{N3}, a complex showing the unexpected coordination of nitrogen adjacent to the carboxylate group), (cations shown in Figure 1). Through this family of complexes the utility and versatility of the synthetic route applying $[Ru(CO)_2Cl_2]_n$ as key synthon is further demonstrated. In **3**^{N3}, dipyrido[3,2,-a;2′,3-c]phenazine (dppz) has been incorporated so that in future biosensing applications a change in photochemical response could be induced on intercalation of the complex into oligonucleotides.[30,31] We report the detailed electrochemical and spectroscopic characterization of the complexes together with the X-ray crystal structures of three complexes, $[Ru(bpy)_2(cpp)](PF_6)\cdot 4H_2O$, **1a**, the deprotonated derivative of **1**, **3**^{N3}, and a key precursor, $[Ru^{II}(cppH)(CO)_2Cl_2]\cdot H_2O$.

Experimental Section

Chemicals. $RuCl_3\cdot xH_2O$ (Pressure Chemicals) and all other chemicals were of reagent or analytical grade and used as obtained

(12) Balzani, V.; Credi, A.; Venturi, M. *Coord. Chem. Rev.* **1998**, *171*, 3–16.
(13) Balzani, V.; Barigelletti, S.; Belser, P.; Campagna, S.; Juris, A.; Von Zelewsky, A. *Coord. Chem. Rev.* **1988**, *84*, 85–277; and references therein.
(14) O'Regan, B.; Gratzel, M. *Nature* **1991**, *335*, 737–740.
(15) Verheijen, J. C.; Van der Marel, G. A.; Van Boom, J. H.; Metzler-Nolte, N. *Bioconjugate Chem.* **2000**, *11*, 741–743.
(16) Telser, J.; Cruickshank, K. A.; Schanze, K. S.; Netzel, T. L. *J. Am. Chem. Soc.* **1989**, *111*, 7221–7226.
(17) Khan, S. I.; Beilstein, A. E.; Grinstaff, M. W. *Inorg. Chem.* **1999**, *38*, 418–419.
(18) Mitra, D.; Di Cesare, N.; Sleiman, H. F. *Angew. Chem., Int. Ed.* **2004**, *43*, 5804–5808.
(19) Hess, A.; Metzler-Nolte, N. *Chem. Commun.* **1999**, 885–886.
(20) Nazeeruddin, M. K. P.; Zakeeruddin, S. M.; Lagref, J.-J.; Liska, P.; Comte, P.; Barolo, C.; Viscardi, G.; Schenk, K.; Gratzel, M. *Coord. Chem. Rev.* **2004**, *248*, 1317–1328.
(21) Kepert, C. M.; Deacon, G. B.; Spiccia, L. *Chem. Coord. Rev.* **2004**, *248*, 1329–1341; and references therein.
(22) Deacon, G. B.; Kepert, C. M.; Sahely, N.; Skelton, B. W.; Spiccia, L.; Thomas, N. C.; White, A. H. *J. Chem. Soc., Dalton Trans.* **1999**, 275–277.
(23) Kepert, C. M.; Bond, A. M.; Deacon, G. B.; Spiccia, L.; Skelton, B. W.; White, A. H. *J. Chem. Soc., Dalton Trans.* **2004**, 1766–1774.
(24) Kepert, C. M.; Deacon, G. B.; Sahely, N.; Spiccia, L.; Fallon, G. D.; Skelton, B. W.; White, A. H. *Inorg. Chem.* **2004**, *43*, 2818–2827.
(25) Black, D. S. C.; Deacon, G. B.; Thomas, N. C. *Aust. J. Chem.* **1982**, *35*, 2445–2453.
(26) Nickita, N.; Bhatt, A. I.; Bond, A. M.; Deacon, G. B.; Gasser, G.; Spiccia, L. *Inorg. Chem.* **2007**, *46*, 8638–8651.
(27) Casalboni, F.; Mulazzani, Q. G.; Clark, C. D.; Hoffman, M. Z.; Orizondo, P. L.; Perkovic, M. W.; Rillema, D. P. *Inorg. Chem.* **1997**, *36*, 2252–2257.
(28) Rillema, D. P.; Blanton, C. B.; Shaver, R. J.; Jackman, D. C.; Boldaji, M.; Bundy, S.; Worl, L. A.; Meyer, T. J. *Inorg. Chem.* **1992**, *31*, 1600–1606.
(29) Clark, C. D.; Hoffman, M. Z.; Rillema, D. P.; Mulazzani, Q. G. *J. Photochem. Photobiol., A* **1997**, *110*, 285–290.
(30) Bhattarcharya, P. K.; Barton, J. K.; Delaney, S.; Paschaly, M. *Inorg. Chem.* **2002**, *41*, 1966–1974.
(31) Erkkila, K. E.; Odom, D. T.; Barton, J. K. *Chem. Rev.* **1999**, *99*, 2777–2796.

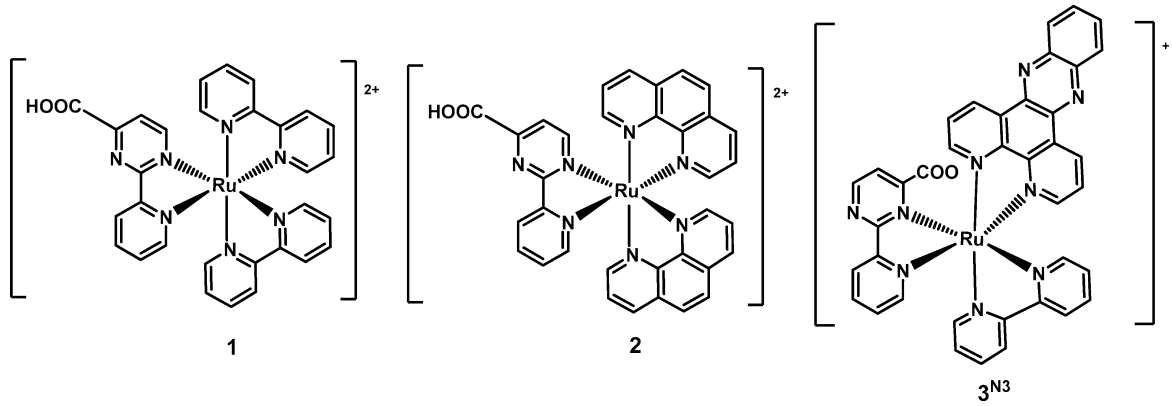

Figure 1. Structures of $\mathbf{1}-\mathbf{3}^{N3}$.

from commercial suppliers. Dipyrido[3,2,-a;2′,3-c]phenazine was synthesized by literature procedures.[32,33] HPLC grade CH_3CN (Merck) was used for all spectral and electrochemical studies. Tetrabutylammonium hexafluorophosphate ($^nBu_4NPF_6$, Fluka) was recrystallized from acetone prior to use as the electrolyte for the electrochemical studies in CH_3CN.[34]

Instrumentation and Methods. Thin layer chromatography (TLC) was performed using silica gel 60 F-254 (Merck) plates followed by preparative column chromatography on silica gel. Concentration of the eluents from the column chromatography was achieved under reduced pressure at 60 °C. ^1H NMR and $^1H-^1H$ spectra were recorded on either a 300 or 400 MHz Bruker NMR spectrometers. The chemical shifts, δ, were calibrated using either tetramethylsilane (TMS) or signals due to the residual protons of deuterated solvents. UV−visible spectra were recorded on Varian Cary 3 or Cary 5G spectrophotometers. For spectroelectrochemical experiments, the samples were prepared in CH_3CN with a supporting electrolyte present (0.1 M Bu_4NPF_6) and carried out using an EG&G PAR model 273 potentiostat. These experiments were performed with approximately 2 mL of solution containing 0.1−0.3 mM of the analyte in CH_3CN. Luminescence emission spectra were obtained following excitation at 450 nm using a Varian Fluorescence spectrometer equipped with a 250 W xenon lamp as an excitation source. These measurements were carried out in acetonitrile solution at room temperature in a 10 mm quartz cuvette using complex concentrations of 10 μM. Emission spectra were absorbance matched and corrected for variations in PMT responses. IR spectra measured on KBr disks were recorded with a Perkin-Elmer FTIR 1600 series spectrometer. Mass spectra were recorded using a Micromass Platform *II* instrument with an ESI source. The capillary voltage was set at 3.5 eV and the cone voltage at 35−50 V. Elemental analysis was performed by the Campbell Microanalytical Laboratory, University of Otago, NZ.

Electrochemical Measurements. Voltammetric measurements in acetonitrile were performed over the scan rate range of 0.002−1 V s^{-1} using either a BAS100 (Bioanalytical Systems) or a VoltaLab PGZ301 (Radiometer Analytical) electrochemical workstation.[35] Oxygen was removed from the acetonitrile solutions by purging the solutions with high purity nitrogen. A typical three electrode cell was employed which was composed of a platinum working electrode (0.0079 cm^2), a large surface area Pt counter electrode, and an $Ag/AgNO_3$/MeCN (0.1 M $AgNO_3$) reference electrode. Rotated disk voltammetry at rates from 500−3000 rpm utilized a platinum disk working electrode having an area of 0.071 cm^2 and rotated with a Metrohm 628−10 assembly. The potential of the reference electrode was calibrated against the ferrocene/ferrocinium (Fc/Fc^+) redox couple by monitoring the reversible potential for oxidation of ferrocene under the same conditions used to carry out the voltammetry of the ruthenium(II) complexes. All electrochemical experiments were carried out at (20 ± 2) °C inside a Faraday cage under a nitrogen atmosphere and with 0.1 M Bu_4NPF_6 present as the supporting electrolyte. The working electrodes were polished with an aqueous aluminum oxide slurry (0.3 μm), then rinsed with acetone, and dried before each voltammetric experiment. Optically transparent thin-layer electrolysis (OTTLE) experiments were carried out using an EG&G PAR model 273 potentiostat. The OTTLE experiments were performed with approximately 2 mL of solution containing 0.1−0.5 mM of the analyte in CH_3CN.

$[Ru(CO)_2Cl_2]_n$, $[Ru(bpy)_2Cl_2]$, $[Ru(bpy)(CO)_2Cl_2]$, and $[Ru(bpy)(CO)Cl_2]_2$. These compounds were prepared according to literature methods.[22,25,36] The IR spectra of these compounds and ^1H NMR spectrum of $[Ru(bpy)_2(CO)_2Cl_2]$ were in agreement with the literature reports. Elemental analysis also confirmed the formation of $[Ru(bpy)_2Cl_2]$.

2-Picolinimidamide Hydrochloride. Sodium metal (0.50 g, 0.022 mol) was reacted with methanol (200 mL) to form a solution of sodium methoxide. 2-Cyanopyridine, pyCN, (26.7 g, 0.26 mol) was added, and the mixture was stirred until a homogeneous solution was formed, then left to stand for 16 h. Ammonium chloride (11.0 g, 0.28 mol) was then added to the solution and stirred at room temperature for 6 h, after which the mixture was filtered to remove any unreacted NH_4Cl and the filtrate was taken to dryness under high vacuum. The solid residue was triturated with diethyl ether a few times to remove any unreacted pyCN. After each trituration, the solid residue was collected by filtration and dissolved in 40 mL of hot absolute ethanol. An insoluble white precipitate remained in the ethanol solution consisting mainly of unreacted NH_4Cl. The NH_4Cl was removed by filtration, and diethyl ether was added to the filtrate to initiate crystallization of the product. After standing for 2 h and cooling to 4 °C, a white precipitate of 2-picolinimidamide hydrochloride was collected. (Yield, 22.0 g, 54%).

(32) Peek, B. M.; Ross, G. T.; Edwards, S. W.; Meyer, G. J.; Meyer, T. J.; Erickson, B. W. *J. Pept. Protein. Res.* **1991**, *38*, 114–123.
(33) Dickeson, J. E.; Summers, L. A. *Aust. J. Chem.* **1970**, *23*, 1023–1027.
(34) Kissinger, T.; Heineman, W. R. *Laboratory Techniques in Electroanalytical Chemistry*, 2nd ed.; Marcel Dekker Inc.: New York, 1996; pp 469−486.
(35) Wolfbauer, G.; Bond, A. M.; Deacon, G. B.; MacFarlane, D. R.; Spiccia, L. *J. Am. Chem. Soc.* **2000**, *122*, 130–142.
(36) Anderson, P. A.; Deacon, G. B.; Haarmann, K. H.; Keene, F. R.; Meyer, T. J.; Reitsma, D. A. N.; Skelton, B. W.; Strouse, G. F.; Thomas, N. C.; Treadway, J. A.; White, A. H. *Inorg. Chem.* **1995**, *34*, 6145–6157.

Selected IR bands (KBr), υ/cm^{-1}: 3038 m, 1894 s, 1590 m, 1531 s, 1466 m, 1427 m, 1100 m, 997 s, 806 s. ^{1}H NMR (D_2O), δ ppm: 8.84 (m, 1H, H6′); 8,17 (m, 2H, H4′ and H5′); 7.84 (m, 1H, H3′). ES mass spectrum (m/z) (positive mode): 122.0 $[M + H]^+$ (100%).

4-Methyl-2-(2′-pyridyl)pyrimidine, mpp. Sodium metal (5.03 g, 0.22 mol) was reacted with absolute ethanol (200 mL) to form sodium ethoxide. 2-Picolinimidamide hydrochloride (26.1 g, 0.17 mol) was then added to this solution. Acetylacetaldehyde dimethyl acetal (26.5 mL, 0.20 mol) was subsequently added to the solution at which point the solution turned orange. The reaction mixture was refluxed for 4 h, followed by stirring overnight at room temperature. Sodium chloride was precipitated during the reaction and removed by filtration. Glacial acetic acid (5.70 mL) was added to the filtrate, and the excess solvent removed under high vacuum, leaving behind a dark yellow residue. The residue was taken to dryness under vacuum for 24 h. The residue was purified using Soxhlet extraction with ether for 3 h. The filtrate containing the desired product was kept aside while the remaining residue in the thimble was sonicated with dichloromethane. Undissolved material from the sonication was filtered off, and the dichloromethane solution combined with the ether filtrate was concentrated via rotary evaporation. Hexane (20 mL) was added to the solution to initiate crystallization. The pale yellow crystals of the desired product were collected on a sinter lined glass funnel and air-dried. (Yield, 8.12 g, 28%).

Selected IR bands (KBr), υ/cm^{-1}: 1567 s, 1557s, 1455 m, 1424 s, 1387 m, 1249 m, 1134 m, 1091 w, 1100 m, 993 s, 838 m, 773 s. ^{1}H NMR (C DCl$_3$), δ ppm: 8.79 (d, ^3J = 4.2 Hz, 1H, H6′); 8.75 (d, ^3J = 5.1 Hz, 1H, H6); 8.53 (dd, ^3J = 5.0 Hz, 1H, H4′); 7.90 (dd, ^3J = 5.0 Hz, ^4J = 1.0 Hz, 1H, H3′); 7.42 (m, 1H, H5′); 7.17 (d, ^3J = 5.1 Hz, 1H, H5); 2.67 (s, 3H, CH_3). ES mass spectrum (m/z) (positive mode): 171.9 $[M + H]^+$ (100%).

2-Pyridyl-2-pyrimidine-4-carboxylic Acid·HNO$_3$, cppH·HNO$_3$. 4-Methyl-2-(2-pyridyl) pyrimidine (1.13 g, 6.6 mmol) was dissolved in 7.5 mL of 1:1 (v/v) ratio of concentrated nitric acid:distilled water. Concentrated hydrochloric acid (8 drops) was added to the solution, and this solution was refluxed at 100 °C. Once brown fumes had ceased to evolve, another 0.5 mL of concentrated nitric acid were added, and the reflux was continued for 7 h. The resulting solution was cooled in an ice bath and crystallization immediately began. After storage at 4 °C overnight, the resulting pale yellow crystals were collected via filtration and washed with cold water, followed by methanol. (Yield, 1.67 g, 96%).

Anal. Found (%): C; 45.1; H, 3.2; N, 21.5. Calcd for $C_{10}H_8N_4O_5$ (%): C, 45.4; H, 3.1; N, 21.2. Selected IR bands (KBr), υ/cm^{-1}: 3072 w, 2643 br, 1740 s, 1700 s, 1625 s, 1573 s, 1536 m, 1474 m, 1415 m, 1299 m, 1029 s, 997 w, 876 w, 820 m, 769 s, 722 s. ^{1}H NMR (D_2O), δ ppm: 8.93 (dd, ^3J = 5.5 Hz, ^4J = 0.9 Hz, 1H, H6); 8.58 (d, ^3J = 5.9 Hz, 1H, H6′); 8.26 (dd, ^3J = 5.5 Hz, ^4J = 0.9 Hz, 1H, H5); 7.93 (dd, ^3J = 5.9 Hz, ^4J = 1.0 Hz, 1H, H4′); 7.80 (d, ^3J = 5.9 Hz, 1H, H3′); 7.48 (m, 1H, H5′). ES mass spectrum (m/z) (positive mode): 202.1 $[M + H]^+$ (100%), 224.2 $[M + Na]^+$ (73%).

[Ru^{II}(cppH)(CO)$_2$Cl$_2$]·H$_2$O. CppH·HNO$_3$ (0.71 g, 2.7 mmol) was suspended in 25 mL of MeOH under a stream of nitrogen at 60 °C. After 10 min, $[Ru^{II}(CO)_2Cl_2]_n$ (0.50 g, 2.2 mmol) was added to the solution. The mixture was refluxed at the same temperature for 20 min. This resulted in the dissolution of the $[Ru^{II}(CO)_2Cl_2]_n$ followed by precipitation of the product. The mixture was cooled to 2 °C to complete the precipitation. The resulting pale yellow colored solid, $[Ru^{II}(cppH)(CO)_2Cl_2]\cdot H_2O$, was collected, washed with cold MeOH and dried in vacuo (Yield, 0.76 g, 62%). Single crystals of $[Ru^{II}(cppH)(CO)_2Cl_2]\cdot H_2O$ suitable for X-ray crystallography, grew from methanol over a period of 1 week.

Anal. Found (%): C, 32.6; H, 2.0; N, 9.4. Calcd. for $C_{12}H_9Cl_2N_3O_5Ru$ (%): C, 32.2; H, 2.0; N, 9.4. Selected IR bands (KBr), υ/cm^{-1}: 3096 w, 2757 w (br), 2068 s, 2013 s, 1744 m, 1618 w, 1578 w, 1554 w, 1426 m, 1251 w, 1208 w, 1026 w, 820 w, 766 m. ^{1}H NMR (DMSO-d_6), δ ppm: 9.81 (d, 1H, ^3J = 5.8 Hz, H6); 9.29 (m, 1H, H6′); 8.85 (m, 1H, ^3J = 5.8 Hz, H5); 8.47 (m, 1H, H4′); 8.17 (m, 1H, H3′); 8.03 (m, 1H, H5′). ES mass spectrum (m/z) (negative mode): 429.8 $[(Ru^{II}(cpp)(CO)_2Cl_2)]^+$;$(M - H)^-$].

[Ru^{II}(bpy)$_2$(cppH)](PF$_6$)$_2$·H$_2$O (1·H$_2$O). Method 1. $[Ru^{II}(bpy)_2Cl_2]$ (0.42 g, 0.9 mmol) and cppH (0.22 g, 1.1 mmol) were added to degassed EtOH (95%, 50 mL). The initially purple mixture was refluxed for 6.5 h under N_2 resulting in an orange solution. The reaction mixture was stored at 4 °C for 4 days resulting in red crystals of $[Ru^{III}(bpy)_2Cl_2]Cl\cdot H_2O$ (Yield, 0.13 g, 29%), confirmed by a unit cell determination.[37] The crystals were filtered, the filtrate was evaporated to dryness under vacuum, and the residue was dissolved in water. The solution was filtered to remove any insoluble impurities, and the aqueous filtrate was treated with aqueous KPF_6 (0.1 M, 20 mL) instantly resulting in a red suspension. A dark red microcrystalline product was collected by filtration, $[Ru^{II}(bpy)_2(cppH)](PF_6)_2\cdot H_2O$ (**1·H$_2$O**, Yield, 0.16 g, 21%). Single crystals of $[Ru^{II}(bpy)_2(cpp)](PF_6)\cdot 4H_2O$ suitable for X-ray crystallography, **1a**, grew in the aqueous filtrate containing **1·H$_2$O** over 2 months (Yield, 0.02 g, 3%). (Total yield, 0.18 g, 24%). Anal. for **1·H$_2$O**. Found (%): C, 39.1; H, 3.1; N, 10.6. Calcd. for $C_{30}H_{25}F_{12}N_7O_3P_2Ru$ (%): C, 39.1; H, 2.7; N, 10.5. IR bands (KBr), υ/cm^{-1}: 3085 m, 1925 m, 1736 w, 1719 w, 1701 w, 1605 s, 1449 s, 1317 m, 1246 m, 1165 m, 1030 m, 839 s, 764 s. ^{1}H NMR (DMSO-d_6), δ ppm: 8.83 (m, 4H); 8.15−8.27 (m, 6H,); 8.05 (d, 1H, ^3J = 4.8 Hz); 7.92 (d, ^3J = 5.8 Hz, 1H); 7.65−7.79 (m, 5H); 7.43−7.57 (m, 5H). ES mass spectrum (m/z) (positive mode): 307.5 ($[Ru^{II}(bpy)_2(cppH)]^{2+}$, (M^{2+})), 570 ($[Ru^{II}(bpy)_2(C_9H_6N_3^-)]^+$), 615 ($[Ru^{I}(bpy)_2(cppH)]^+$, $(M)^+$).

[Ru^{II}(bpy)$_2$(cppH)](PF$_6$)$_2$ (1). Method 2. 2,2′-Bipyridine (0.39 g, 2.5 mmol) and an excess of Me_3NO (0.35 g, 4.7 mmol) were added to a solution of $[Ru^{II}(cppH)(CO)_2Cl_2]\cdot H_2O$ (0.41 g, 1.0 mmol) in 25 mL of deoxygenated 2-methoxyethanol. This solution was refluxed at 120 °C for 3 h. After cooling the solution to room temperature, the solvent was removed via rotary evaporation, and the crude product purified by column chromatography on silica gel (eluent CH_3CN/H_2O/aqueous saturated solution of KNO_3, 10:3:1 v/v). The darkest band was collected and solvent removed under reduced pressure. The residue was suspended in MeCN to dissolve the complex and to separate it from the insoluble KNO_3. After filtration, MeCN was removed via rotary evaporation, and the product was redissolved in 15 mL of water. An aqueous solution of HPF_6 (60%) solution was added dropwise, until no further precipitation was observed, to give dark red microcrystals. The crystals were collected by filtration, washed with ether, and dried under high vacuum to give **1** as a dark red solid. (Yield, 0.39 g, 43%).

Anal. Found (%): C, 39.9; H, 3.2; N, 10.8. Calcd. for $C_{30}H_{23}F_{12}N_7O_2P_2Ru$ (%): C, 39.8; H, 2.6; N, 10.8. IR bands (KBr), υ/cm^{-1}: 1720 m, 1689 m, 1645 s, 1546 s, 1423 vs, 1243 m, 1152 m, 843 vs UV−visible (MeCN) [λ_{max} (nm); (ε_{max}) (M^{-1} cm^{-1}): 242 (28 500), 283 (63 800), 422 (10 100), 450 (11 400). ^{1}H NMR (C D_3CN), δ ppm: 8.89 (d, 1H, ^3J = 5.9 Hz); 8.49−8.53 (m, 4H); 8.22 (d, 1H, ^3J = 5.1 Hz); 8.05−8.16 (m, 5H); 7.89 (d, 1H, ^3J =

(37) Eggleston, D. S.; Goldsby, K. A.; Hdgson, D. J.; Meyer, T. J. *Inorg. Chem.* **1985**, *24*, 4573–4580.

5.9 Hz); 7.85 (d, 1H, $^3J = 5.9$ Hz); 7.70−7.78 (m, 4H); 7.57 (ddd, 1H, $^3J = 5.9$ Hz and $^4J = 1.5$ Hz); 7.40−7.45 (m, 4H). ES Mass Spectrum (*m*/*z*) (positive mode): 307.5 $[[Ru^{II}(bpy)_2(cppH)]^{2+}; (M^{2+})]$.

$[Ru^{II}(phen)_2(cppH)](PF_6)_2 \cdot 2H_2O$ (2). This complex was prepared in the same manner as $[Ru^{II}(bpy)_2(cppH)](PF_6)_2$ (**1**) using method 2, but using $Ru^{II}(cppH)(CO)_2Cl_2 \cdot H_2O$ (0.55 g, 1.3 mmol), 1,10-phenanthroline (0.59 g, 3.3 mmol), and an excess of Me_3NO (0.33 g, 4.5 mmol). The crude product was purified by column chromatography on silica gel (eluent CH_3CN/H_2O/aqueous saturated solution of KNO_3, 10:3:1 v/v). The darkest band was collected and solvent removed under reduced pressure. The residue was suspended in MeCN to dissolve the complex and to separate it from the insoluble KNO_3. After filtration, MeCN was removed via rotary evaporation, and the product was redissolved in 15 mL of water. An aqueous solution of HPF_6 (60%) was added dropwise, until no further precipitation was observed, to give a dark red solid. The crystals were collected by filtration, washed with ether, and dried under high vacuum to give **$2 \cdot H_2O$** as a red solid. (Yield, 0.67 g, 54%).

Anal. Found (%): C, 41.6; H, 2.9; N, 9.6. Calcd. for $C_{34}H_{27}F_{12}N_7O_4P_2Ru$ (%): C, 41.3; H, 2.8; N, 9.9. IR bands (KBr), υ/cm^{-1}: 2366 w, 2026w, 1716 w, 1685 w, 1637 w, 1618 s, 1427 w, 1410 w, 1376 s, 1244 w, 1147s, 1086 s, 846 s, 720 w. UV−visible (CH_3CN) [λ_{max} (nm); (ε_{max}) (M^{-1} cm^{-1}): 222 (47 900), 263 (70 900), 382 (9 700), 419 (11 300), 448 (12 100). ^{1}H NMR (C D_3CN), δ ppm: 8.91 (d, 1H, $^3J = 6.5$ Hz); 8.67−8.70 (m, 2H); 8.56−8.59 (m, 2H); 8.36 (d, 1H, $^3J = 4.3$ Hz); 8.21−8.29 (m, 5H); 8.10−8.16 (m, 2H); 7.28−7.88 (m, 2H); 7.74−7.78 (m, 3H); 7.70 (dd, 1H, $^3J = 5.5$ Hz, $^3J = 0.9$ Hz), 7.57−7.45−7.58 (m, 2H), 7.33 (m, 1H). ES Mass Spectrum (*m*/*z*) (positive mode): 331.4 $[(Ru^{II}(phen)_2(cppH)^{2+}; (M^{2+})]$, 661.8 $[(Ru^{II}(phen)_2(cpp)]^+;(M - H)^+]$.

$[Ru(bpy)(dppz)(CO)Cl](PF_6) \cdot H_2O$. Dipyrido[3,2,-a;2′,3-c]phenazine (0.26 g, 0.9 mmol) was added to a mixture of $[Ru(bpy)(CO)Cl_2]_2$ (0.28 g, 0.6 mmol) in deoxygenated 2-methoxyethanol (20 mL) under a N_2 atmosphere. This solution was refluxed at 120 °C for 2 h to form a dark orange solution. The solvent was removed in vacuo to yield a pale orange colored solid. This was suspended in distilled H_2O, sonicated for 5 min, cooled to 4 °C and any undissolved solid removed by filtration. The filtrate was mixed with a 1 M aqueous solution of KPF_6 (5 mL) to yield an orange colored solid. This solid was collected by filtration, washed once with H_2O, once with H_2O/EtOH (1:1 v/v) and dried at 70 °C in air (Yield, 0.38 g, 84%).

Anal. Found (%): C, 45.3; H, 2.6; N, 10.8. Calcd. for $C_{29}H_{20}ClF_6N_6O_2PRu$ (%): C, 45.5; H, 2.6; N, 11.0. IR bands (KBr), υ/cm^{-1}: 3082 w, 1979 s, 1604 m, 1542 w, 1496 m, 1471 w, 1449 m, 1422 m, 1360 m, 1314 w, 1243 w, 1122 w, 1080 w, 1056 w, 851 s, 766s, 730 m. ^{1}H NMR (DMSO-d_6), δ ppm: 9.84 (dd, $^3J = 5.3$ Hz, $^3J = 1.3$ Hz, 1H); 9.55−9.57 (m, 2H); 9.49 (d, $^3J = 6.3$ Hz, 1H); 8.91 (d, $^3J = 6.5$ Hz, 1H); 8.74 (d, $^3J = 7.9$ Hz, 1H); 8.55 (ddd, $^3J = 6.5$ Hz, $^4J = 1.5$ Hz, 1H); 8.29−8.31 (m, 1H); 8.10−8.21 (m, 2H); 8.05−8.08 (m, 3H); 7.97−8.03 (m, 3H); 7.84 (d, 1H, $^3J = 4.9$ Hz); 7.34 (ddd, 1H, $^3J = 4.9$ Hz, $^4J = 1.5$ Hz). ES Mass Spectrum (*m*/*z*): 602.9 $[(Ru^{II}(bpy)(dppz)(CO)Cl)^+;(M^+)]$.

$[Ru^{II}(bpy)(dppz)(cpp)](NO_3) \cdot 8H_2O$ (3^{N3}). $CppH \cdot HNO_3$ (0.15 g, 0.6 mmol) and excess Me_3NO (0.17 g, 2.3 mmol) were added to a solution of $[Ru(bpy)(dppz)(CO)Cl](PF_6) \cdot H_2O$ (0.28 g, 0.5 mmol) in deoxygenated 2-methoxyethanol (25 mL) under N_2 atmosphere. The round-bottom flask was covered with aluminum foil, and the solution was refluxed at 120 °C for 3 h under a N_2 in the dark. After cooling to room temperature, the resulting bright orange colored solid that had precipitated was collected by filtration and washed with H_2O, cold ethanol, and diethyl ether successively. The solvent was removed from the filtrate in vacuo to give a viscous red oil, which was suspended in H_2O (25 mL) and sonicated for 5 min. After cooling to 4 °C and filtration, a 1 M aqueous solution of KPF_6 was added dropwise to the filtrate until no further precipitation of the product was observed. The dark red precipitate was collected by filtration and washed with H_2O, cold ethanol, and ether in succession. Both the dark red precipitate and orange solids were purified by column chromatography on silica gel (eluent CH_3CN/H_2O/aqueous saturated solution of KNO_3, 10:3:1 v/v). The darkest band was collected and slow evaporation of this acetonitrile/water mixture deposited some dark red needles of **3^{N3}**, $[Ru(bpy)(dppz)(cpp)](NO_3) \cdot 8H_2O$ (a deprotonated derivative of **3**), that were suitable for X-ray crystallography. Following separation of some of the crystals, the solvent was removed under reduced pressure, and the resulting solid was dissolved in MeCN, separating it from the insoluble KNO_3. The solvent was removed under reduced pressure and the solid was redissolved in water. A 1 M aqueous solution of HPF_6 was then added dropwise until no further precipitation was observed. The dark red microcrystals were collected by filtration and washed with diethyl ether (Yield, 0.18 g, 37%).

Characterization of 3^{N3}. Anal. Found (%): C, 48.5; H, 4.8; N, 14.4. Calcd. for $C_{38}H_{40}N_{10}O_{13}Ru$ (%): C, 48.3; H, 4.3; N, 14.8. IR bands (KBr), υ/cm^{-1}: 1719 w, 1654 w, 1618 s, 1577 w, 1560 w, 1534 w, 1491 w, 1466 w, 1447 w, 1421 w, 1384 s, 1357 w, 1031 m, 1285 w, 1119 w, 1080 w, 815 w, 768 m, 729 w. UV−visible (MeCN) [λ_{max} (nm); (ε_{max}) (M^{-1}. cm^{-1}): 355 (11 600), 445 (10 600). ^{1}H NMR (C D_3CN), δ ppm: 9.65 (d, 1H, $^3J = 6.9$ Hz); 9.46 (d, 1H, $^3J = 6.9$ Hz); 8.84 (d, 1H, $^3J = 5.7$ Hz), 8.80 (d, 1H, $^3J = 5.9$ Hz), 8.66 (d, 1H, $^3J = 5.8$ Hz), 8.43−8.51 (m, 4H); 8.08−8.12 (m, 4H); 7.92−8.06 (m, 3H); 7.85 (ddd, 1H, $^3J = 5.3$ Hz, $^4J = 0.9$ Hz); 7.63−7.68 (m, 2H); 7.55 (ddd, 1H, 1H,$^3J = 5.3$ Hz, $^4J = 1.1$ Hz), 7.45−7.49 (m, 2H); 7.13 (ddd, 1H,$^3J = 5.3$ Hz, $^4J = 1.1$ Hz); 7.05 (d, 1H, $^3J = 5.2$ Hz). ES Mass Spectrum (*m*/*z*) (positive mode): 740.0 $[Ru^{II}(bpy)(dppz)(cpp)]^+$; $(M - H)^+]$, 370.6 $[(Ru^{II}(bpy)(dppz)(cppH)^+; (M)^{2+}]$.

Characterization of Isomer Mixture. Anal. Found (%): C, 51.8; H, 3.6; N, 15.7. Calcd. for $C_{38}H_{32}N_{10}O_9Ru$ (%): C, 52.2; H, 3.7; N, 16.0. IR bands (KBr), υ/cm^{-1}: 1719 w, 1627 s and br, 1581 w, 1492 w, 1466 w, 1447 w, 1421 w, 1395 m, 1377 s, 1358 m, 1031 m, 1285 w, 1119 w, 1080 w, 764 s, 728 w. ^{1}H NMR (C D_3CN), δ ppm: 9.65 (d, 2H, $^3J = 6.9$ Hz); 9.59 (d, 1H, $^3J = 6.7$ Hz); 8.87 (d, 1H, $^3J = 5.5$ Hz), 8.78 (d, 1H, $^3J = 5.6$ Hz), 8.43−8.46 (m, 4H); 8.26 (d, 1H, $^3J = 5.5$ Hz), 7.94−8.12 (m, 12H), 7.67−7.80 (m, 2H), 7.60 (d, 1H, $^3J = 5.6$ Hz), 7.54 (d, 1H, $^3J = 5.3$ Hz), 7.48 (d, 1H, $^3J = 5.4$ Hz), 7.49 (dd, 2H, $^3J = 5.3$ Hz, $^4J = 0.9$ Hz), 7.28 (d, 1H, $^3J = 5.5$ Hz), 7.20, (d, 1H, $^3J = 5.3$ Hz), 6.97 (m, 1H). ES Mass Spectrum (*m*/*z*) (positive mode): 740.0 $[Ru^{II}(bpy)(dppz)(cpp)]^+;(M - H)^+]$, 370.6 $[(Ru^{II}(bpy)(dppz)(cppH)^+;(M)^{2+}]$.

X-ray Crystallography. Intensity data from $[Ru^{II}(cppH)(CO)_2Cl_2] \cdot H_2O$ (0.12 × 0.05 × 0.02 mm), **1a** (0.21 × 0.19 × 0.06 mm) and **3^{N3}** (0.10 × 0.08 × 0.06 mm) crystals were measured at 123 K using either a Nonius Kappa CCD (**1a**) or a Bruker Apex 2 CCD ($[Ru^{II}(cppH)(CO)_2Cl_2] \cdot H_2O$ and **3^{N3}**) diffractometer, fitted with graphite-monochromated Mo Kα radiation (0.71073Å). The data were collected to a maximum 2θ value of 50 ° and processed using the Nonius software (collection and refinement parameters are summarized in Table 1). The structures were solved using direct methods and expanded with standard Fourier routines using the

(38) Sheldrick, G. M. *SHELXS-97*; University of Göttingen: Göttingen, Germany, 1997.

Table 1. Selected Single Crystal X-ray Diffraction Data for $[Ru^{II}(cppH)(CO)_2Cl_2]\cdot H_2O$, **1a**, and $\mathbf{3^{N3}}$

crystal	$[Ru^{II}(cppH)(CO)_2Cl_2]\cdot H_2O$	**1a**	$\mathbf{3^{N3}}$
empirical formula	$C_{12}H_9Cl_2N_3O_5Ru$	$C_{30}H_{30}F_6N_7O_6PRu$	$C_{38}H_{40}N_{10}O_{13}Ru$
M/g mol^{-1}	447.19	830.60	945.81
crystal system	monoclinic	monoclinic	monoclinic
space group	*P*21/*c*	*C*2/*c*	*P*21/*c*
a/Å	15.11(2)	23.954(5)	10.6234(5)
b/Å	8.190(10)	13.640(3)	19.7463(8)
c/Å	13.320(19)	21.072(4)	19.6700(8)
β/deg	111.55(2)	106.02(3)	92.552(2)
V/Å^3	1533(4)	6617(2)	4122.1(3)
Z	4	8	4
T/K	123(2)	123(2)	123(2)
λ/Å	0.71073	0.71073	0.71073
D_c/g cm^{-3}	1.937	1.651	1.550
M (Mo Kα)/mm^{-1}	1.399	0.611	0.463
no. data measured	17591	35618	70673
unique data (R_{int})	4578 (0.0462)	6484(0.1240)	9452 (0.0885)
observed data [$I > 2(\sigma)I$]	3570	6484	7219
final R1, wR2 (obs. data)	0.0343[a], 0.0673[b]	0.0809[a], 0.1568[b]	0.0581[a], 0.1294[b]
final R1, wR2 (all data)	0.0535, 0.0740	0.1345, 0.1754	0.0844, 0.1440
ρ_{min}, ρ_{max}/e Å^{-3}	−0.458, 0.901	−0.472, 0.874	−0.756, 1.075

[a] $R = \sum||F_o| - |F_c||/\sum|F_o|$. [b] $R' = [\sum w(|F_o| - |F_c|)^2/\sum F_o^2]^{1/2}$, where $w = [\sigma^2(F_o)]^{-1}$.

SHELX-97 software.[38] All hydrogens except the hydrogens on the water molecules were placed in idealized positions, and all non-hydrogen atoms were refined anisotropically. The nitrate anion and a water molecule (O8W) in $\mathbf{3^{N3}}$ were disordered. The three oxygens of the nitrate were located in two distinct positions, and their occupancies were refined against each other with the smaller part refining isotropically as an anisotropic refinement failed. O8W was also located in two distinct positions, and their occupancies were refined against each other.

Results and Discussion

Synthesis and Characterization. The synthesis of the new ligand, cppH, is described in Scheme 1. On the basis of previous work, the cyano group on 2-cyanopyridine was successfully converted to an amidine using ammonium chloride and a catalytic amount of sodium methoxide.[39] In the next step, the amidine derivative was converted into derivatized pyridyl-pyrimidine following the work of Kawanishi et al.[40] Cyclization of the amidine derivative involved use of acetylacetaldehyde dimethyl acetal and led to the formation of 4-methyl-2-pyridyl-2-pyrimidine (mpp).[40] The final step involves the simple oxidation of the methyl group on the diimine ligand to generate the desired compound, $cppH\cdot HNO_3$.

The ligand, cppH, and its intermediates were characterized using ^{1}H NMR spectroscopy, electrospray mass spectrometry, IR spectroscopy, and elemental analysis for the final product (see Experimental Section). Electrospray mass spectroscopy confirmed the formation of 2-picolinamidine·HCl, 4-methyl-2-(2-pyridyl) pyrimidine (mpp), and the final compound, the hydronitrate of 2-pyridyl-2-pyrimidine-4-carboxylic acid ($cppH\cdot HNO_3$), with peaks at 122, 172, and 202, respectively, corresponding to $[M + H]^+$. The infrared spectrum of mpp shows a characteristic absorption at 1385 cm^{-1} which is associated with a methyl group (most likely a C-(CH_3) stretch). On oxidation of the methyl group to a carboxylic acid, the IR spectrum showed a loss of the band at 1385 cm^{-1} and generation of a ν(CO) absorption at 1740 cm^{-1}. The ^{1}H NMR spectra of 2-picolinamidine·HCl and mpp have not been reported in the literature and are listed in the Experimental Section. The formation of mpp was readily identified from the presence of a singlet at 2.67 ppm and a doublet at 7.17 ppm in the ^{1}H NMR spectrum attributed to the methyl group and H5, respectively. The absence of this singlet confirmed the formation of $cppH\cdot HNO_3$. The other protons of $cppH\cdot HNO_3$ exhibited resonances at similar chemical shifts to that of mpp.

Initial attempts to synthesize the cation of complex **1**, $[Ru(bpy)_2(cppH)]^{2+}$, involved the treatment of $[Ru^{II}(bpy)_2Cl_2]$ with the cppH ligand in ethanol in an inert atmosphere using a standard method described for the synthesis of complexes of the type $[Ru^{II}(bpy)_2L]^{2+}$.[41] However, the first product that crystallized from the reaction mixture was unexpectedly paramagnetic (from ^{1}H NMR spectra). A unit cell of this product confirmed that the major product was *cis*-$[Ru^{III}(bpy)_2Cl_2]Cl\cdot 2H_2O$ (Scheme 2).[37] The desired complex $\mathbf{1\cdot H_2O}$ was isolated as a monohydrate from the filtrate after removal of $[Ru^{III}(bpy)_2Cl_2)]Cl$, evaporation of ethanol, dissolution of the residue in water, and treatment with aqueous KPF_6. Single crystals of **1a** formed in the aqueous filtrate containing **1** after standing for 2 months (Scheme 2). An X-ray crystal structure determination showed it to be the deprotonated species, $[Ru^{II}(bpy)_2(cpp)](PF_6)\cdot 4H_2O$, in contrast to the bulk sample, which was analyzed as $[Ru^{II}(bpy)_2(cppH)](PF_6)_2\cdot H_2O$.

To avoid the oxidation of Ru^{II} to Ru^{III}, $[Ru^{II}(CO)_2Cl_2]_n$ was used as the precursor based on earlier synthesis of ruthenium(II) complexes bearing monocarboxylate diimine ligands[26] and other related ruthenium(II) complexes[21−25,36,42,43] to generate complex **1**, **2**, and $\mathbf{3^{N3}}$ as shown in Scheme 3. $[Ru^{II}(CO)_2Cl_2]_n$ was reacted with $cppH\cdot HNO_3$ to form $[Ru^{II}(cppH)(CO)_2Cl_2]$. This reaction, see Scheme 3, could lead to the formation of a number of isomers for $[Ru^{II}(cppH)(CO)_2Cl_2]\cdot H_2O$ based on the asymmetry of the cppH ligand and the possible coordination of the nitrogen atom ortho or para to the carboxylate in the cppH ligand, as shown in Figure 2. $[Ru^{II}(cppH)(CO)_2Cl_2]\cdot H_2O$ exhibits only two strong absorptions in the 1900−2100 cm^{-1} region of the IR spectrum (at 2068 cm^{-1} and 2013 cm^{-1}) consistent with the presence of *cis*-coordinated carbonyl groups. The lack of other absorptions in this region led to the conclusion that only one isomer of $[Ru^{II}(cppH)(CO)_2Cl_2]\cdot H_2O$ had formed. Thus, the formation of one isomer for complexes **1** and **2** is also most likely. IR analysis together with the X-ray structure determination of $[Ru^{II}(cppH)(CO)_2Cl_2]\cdot H_2O$ (vide infra), confirmed the formation of the products shown in Scheme 3.

Treatment of $[Ru^{II}(cppH)(CO)_2Cl_2]$ with 2 equiv of bpy in the presence of Me_3NO in 2-methoxyethanol produced

(39) Lafferty, J. L.; Case, F. H. *J. Org. Chem.* **1967**, *32*, 1591.
(40) Kawanishi, Y.; Kitamura, N.; Tazuke, S. *Inorg. Chem.* **1989**, *28*, 2968–2975.
(41) Terpetschnig, E.; Szmacinski, H.; Malak, H.; Lakowicz, J. R. *Biophys. J.* **1995**, *68*, 342.
(42) Thomas, N. C.; Deacon, G. B. *Inorg. Synth.* **1989**, *25*, 107–110.
(43) Black, D. S. C.; Deacon, G. B.; Thomas, N. C. *Inorg. Chim. Acta* **1982**, *65*, L75–L76.

Scheme 2. Formation of $[Ru^{II}(bpy)_2(ccpH)]^{2+}$ by Method 1[a]

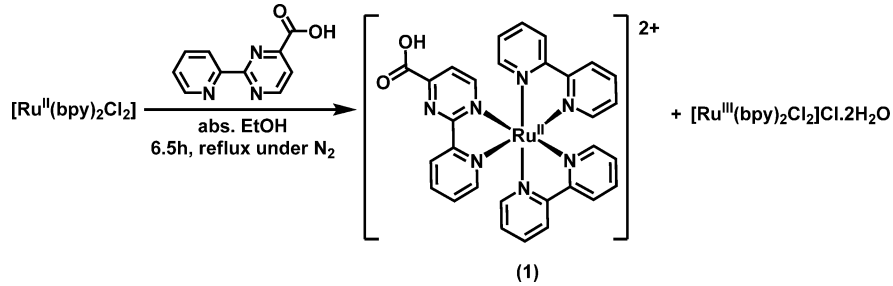

[a] $[Ru^{III}(bpy)_2Cl_2)]Cl \cdot 2H_2O$ is a by-product.

Scheme 3. Synthesis of $\mathbf{1}-\mathbf{3}^{N3}$[a]

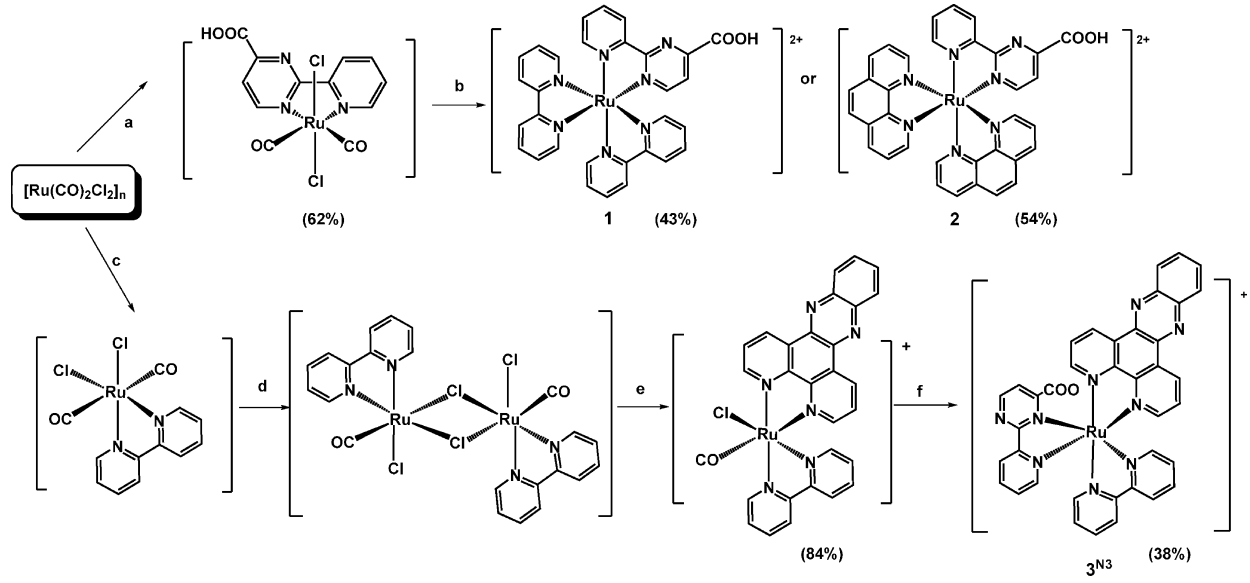

[a] (a) cppH·HNO_3, methanol, reflux, 20 min.; (b) 2 equiv of bpy or phen, excess Me_3NO, 2-methoxyethanol, reflux, 3 h.; (c) bpy, methanol, reflux, 20 min.; (d) hν light, dichloromethane, 48 h; (e) dppz, 2-methoxyethanol, reflux, 2 h; (f) cppH·HNO_3, excess Me_3NO, 2-methoxyethanol, reflux, 3 h.

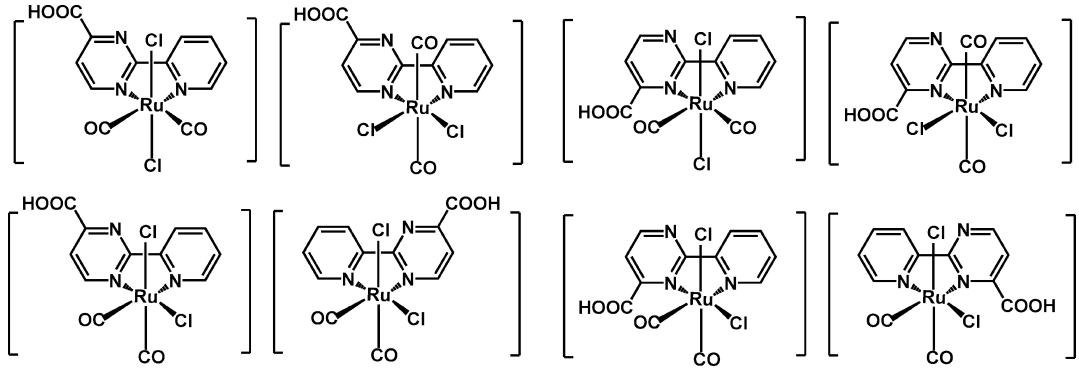

Figure 2. Structures of possible geometric isomers of $[Ru^{II}(cppH)(CO)_2Cl_2] \cdot H_2O$ based on geometry and coordination of either nitrogen atom in the pyrimidine ring of the cppH ligand to ruthenium(II).

$[Ru^{II}(bpy)_2(cppH)](PF_6)_2$ (**1**), after work-up and addition of an aqueous KPF_6 solution. Use of 2 equiv of 1,10-phenanthroline (phen) instead of bpy yielded $[Ru^{II}(phen)_2(cppH)](PF_6)_2$ (**2**). The crystal structure of the precursor $[Ru^{II}(cppH)(CO)_2Cl_2] \cdot H_2O$, together with analysis of its ^1H NMR and IR spectra, provided valuable clues on the coordination mode of cppH in **1** and **2**. The evidence indicates that the nitrogen atom trans to the carboxylate in the cppH ligand is involved in the coordination to the ruthenium(II) center.

In the synthesis of $\mathbf{3}^{N3}$ (Scheme 3), dppz was chosen as the second ligand in the sequential addition of the three dissimilar ligands to ruthenium(II) since $[Ru^{II}(bpy)(dppz)(CO)Cl]^+$ can form fewer isomers in comparison to $[Ru^{II}$-

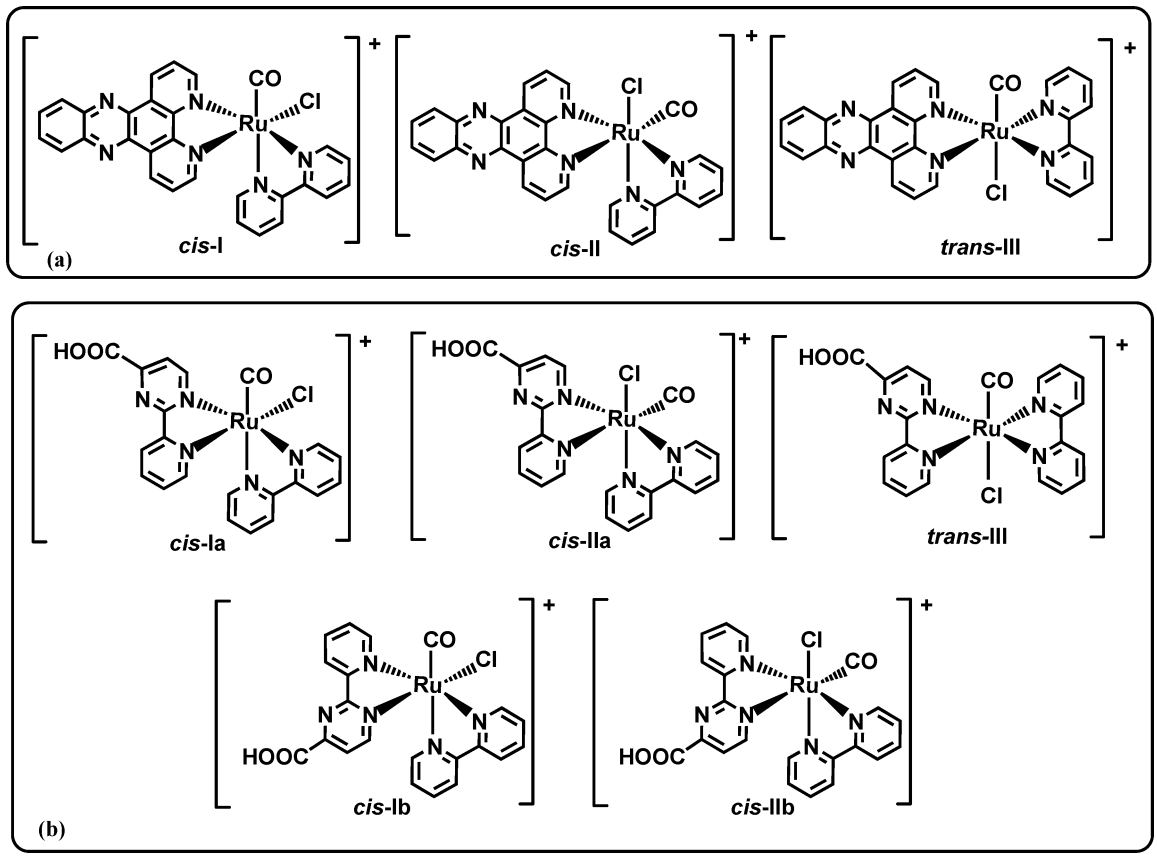

Figure 3. Possible isomers of (a) $[Ru^{II}(bpy)(dppz)(CO)Cl]^+$ and (b) $[Ru^{II}(bpy)(cppH)(CO)Cl]^+$.

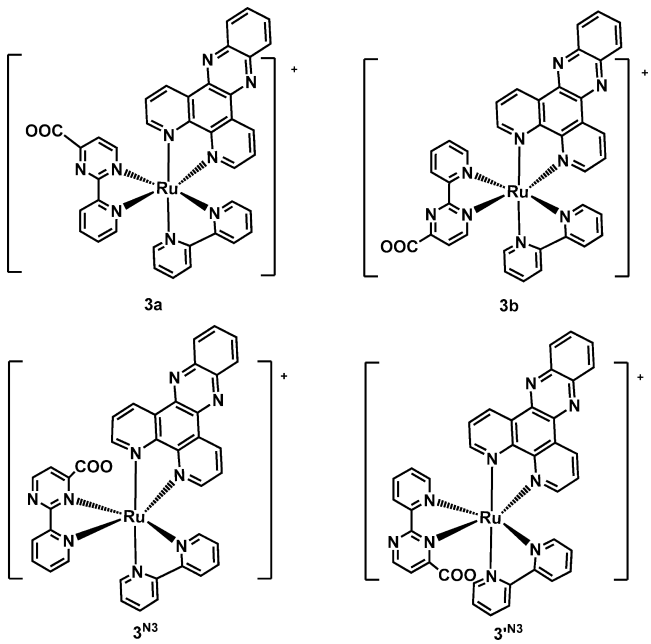

Figure 4. Possible structures of isomers of tris(heteroleptic)ruthenium(II) complex based on coordination of any nitrogen atom of the cpp^- ligand to ruthenium(II).

$(bpy)(cppH)(CO)Cl]^+$ (see Figure 3). The large number of possible isomers of $[Ru^{II}(bpy)(cppH)(CO)Cl]^+$ is a result of the asymmetry of the cppH ligand, as is the case for $[Ru^{II}(bpy)(Mebpy\text{-}COOH)(CO)Cl]^+$.[26] Other derivatives of $[Ru^{II}(bpy)(cppH)(CO)Cl]^+$, not illustrated in Figure 3, may also arise from deprotonation of the carboxylic acid group in cppH and coordination of the nitrogen ortho to the carboxylate. An advantage of preparing $[Ru^{II}(bpy)(dppz)(CO)Cl]^+$ is that the major isomer formed in the second step of the synthesis of the tris(heteroleptic) ruthenium(II) complex can be easily identified based on the cleavage of $[Ru^{II}(bpy)(CO)Cl_2]_2$ and from the small number of possible isomers that can form.

As noted previously for the corresponding Mebpy-COOH complex,[26] $[Ru(bpy)(Mebpy\text{-}COOH)(CO)(Cl)]^+$, separation of the two geometric isomers of $[Ru^{II}(bpy)(dppz)(CO)Cl](PF_6)\cdot H_2O$ based on the method of Keene et al.[44,45] was unsuccessful. The presence of two isomers was established from the ^1H NMR spectrum of $[Ru^{II}(bpy)(dppz)(CO)Cl]^+$ as two sets of resonances corresponding to the dppz and bpy protons were observed (^1H NMR spectrum provided in the Supporting Information). Peak integration was used to establish that 60% of the crude product comprises the major isomer. Cleavage of the dimer, $[Ru(bpy)(CO)Cl_2]_2$, could result in the *cis*-I, *cis*-II, and *trans*-III isomers (Figure 3). Formation of the *cis*-I and *trans*-III isomers is unfavorable, as it would involve ligand dissociation. The major isomer of $[Ru^{II}(bpy)(dppz)(CO)Cl]^+$ that arises from bridge splitting of $[Ru^{II}(bpy)(CO)Cl_2]_2$ is expected to have a *cis*-II arrangement where the bpy nitrogen is *trans* to a terminal chloride ligand (Scheme 3).[22]

(44) Fletcher, N. C.; Keene, F. R. *J. Chem. Soc., Dalton Trans.* **1998**, 2293–2301.
(45) Fletcher, N. C.; Junk, P. C.; Reitsma, D. A.; Keene, F. R. *J. Chem. Soc., Dalton Trans.* **1998**, 133–138.

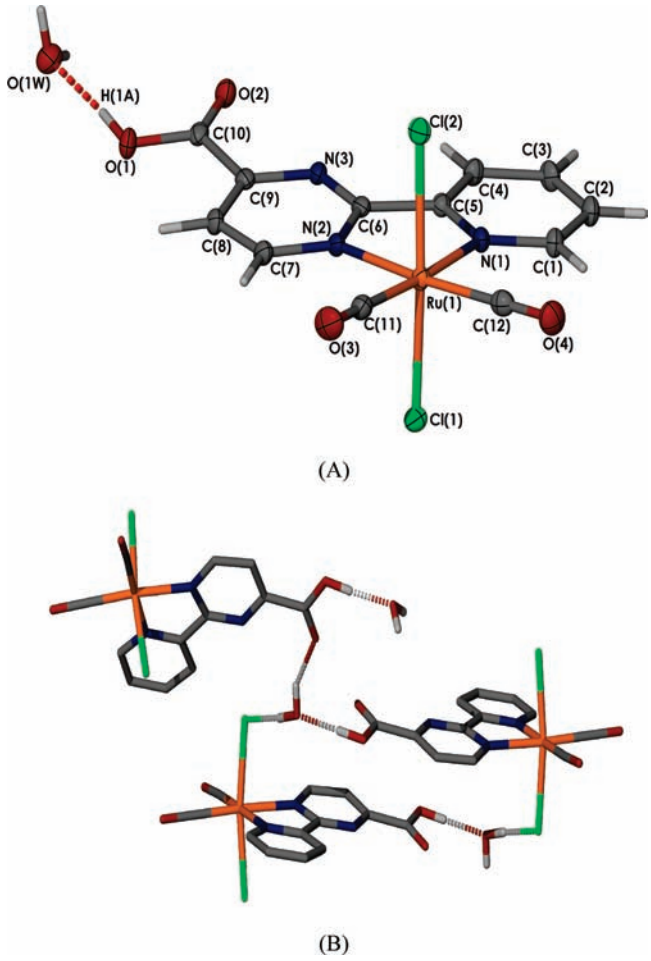

Figure 5. (A) Thermal ellipsoid representation of $[Ru^{II}(cppH)(CO)_2(Cl)_2]\cdot H_2O$ (ellipsoids drawn at 50% probability) and (B) hydrogen bonding interactions involving the water of crystallization in $[Ru^{II}(cppH)(CO)_2(Cl)_2]\cdot H_2O$.

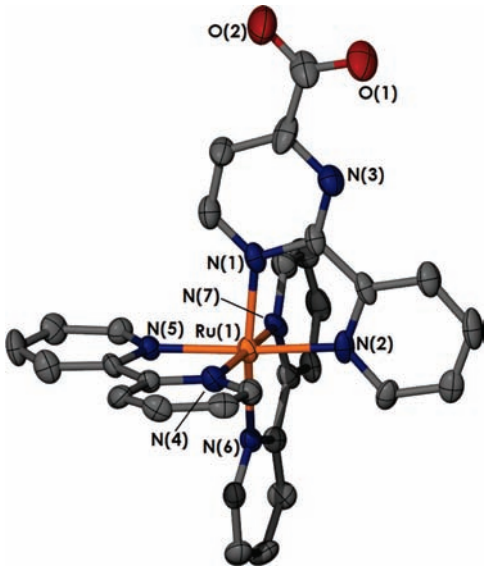

Figure 6. Thermal ellipsoid representation of the cationic unit $[Ru(bpy)_2(cpp)]^+$, **1a** (probability ellipsoids drawn at 50%; hydrogen atoms and solvent molecules omitted for clarity).

Chemical decarbonylation of $[Ru^{II}(bpy)(dppz)(CO)Cl]^+$ in the presence of cppH gave a complicated mixture of geometric isomers of the tris(heteroleptic) ruthenium(II) complex, **3**, as established from the ^{1}H NMR spectrum of the crude product. Crystals of one isomer, $\mathbf{3}^{N3}$, suitable for X-ray crystallography were obtained on slow evaporation of one fraction collected during chromatographic purification (See Experimental Section). A second band collected from this purification contained a mixture of two isomers which could not be separated via crystallization or further chromatography. Complex $\mathbf{3}^{N3}$ was the major product (38% yield) while the isomer mixture was obtained in 27% yield.

Table 2. Selected Bond Lengths [Å] and Angles [deg] for $[Ru^{II}(cppH)(CO)_2Cl_2]\cdot H_2O$[a]

$[Ru^{II}(cppH)(CO)_2Cl_2]\cdot H_2O$	
Ru(1)−C(11)	1.869(3)
Ru(1)−C(12)	1.873(4)
Ru(1)−N(1)	2.084(3)
Ru(1)−N(2)	2.099(3)
Ru(1)−Cl(1)	2.377(2)
Ru(1)−Cl(2)	2.360(3)
C(11)−O(3)	1.127(3)
C(12)−O(4)	1.129(4)
Cl(1)−Ru(1)−Cl(2)	171.23(3)
Cl(1)−Ru(1)−N(1)	88.23(10)
Cl(1)−Ru(1)−N(2)	87.08(12)
Cl(1)−Ru(1)−C(11)	94.08(11)
Cl(1)−Ru(1)−C(12)	94.09(13)
Cl(2)−Ru(1)−N(1)	85.89(10)
Cl(2)−Ru(1)−N(2)	85.31(12)
N(1)−Ru(1)−N(2)	77.57(9)
N(1)−Ru(1)−C(11)	176.24(10)
N(1)−Ru(1)−C(12)	96.66(11)
N(2)−Ru(1)−C(11)	99.56(11)
N(2)−Ru(1)−C(12)	174.09(10)
C(11)−Ru(1)−C(12)	86.15(12)
Ru−C(11)-O(11)	176.5(2)
Ru−C(12)-O(12)	180.0(3)
O(1)−C(10)−O(2)	124.4(3)

[a] esd in parenthesis.

The X-ray crystal structure of $\mathbf{3}^{N3}$ (vide infra) revealed the unusual coordination of the nitrogen atom adjacent to the carboxylate group in the cpp^- ligand. This group was expected to be oriented away from the ruthenium(II) center, as shown in Figure 4 (**3a, 3b**). This unexpected coordination confirms that either heterocyclic nitrogen can coordinate to the metal center and, consequently, four geometric isomers are possible for the tris(heteroleptic) ruthenium(II) complexes of cpp^- (Figure 4), but $\mathbf{3}^{N3}$ prevails.

Investigations were carried out to determine whether the final distribution of the tris(heteroleptic) ruthenium(II) complex varied with reaction conditions. A variety of different reaction conditions, including the use of different solvents (methanol vs 2-methoxyethanol at reflux) and reaction times (3−24 h), were trialled, but there was only a small variation in the distribution of products ($\mathbf{3}^{N3}$ 32−37%, other isomers, 23−29%). Further details of the characterization of all ruthenium(II) compounds, can be found in the Experimental Section and the Supporting Information.

X-ray Crystal Structure Determinations. The X-ray crystal structures of $[Ru^{II}(cppH)(CO)_2Cl_2]\cdot H_2O$, **1a**, and $\mathbf{3}^{N3}$ are shown in Figures 5−7, and selected bond lengths and angles given in Tables 2, 3.

Crystals of $[Ru^{II}(cppH)(CO)_2Cl_2]\cdot H_2O$ were found to be monoclinic, and the crystallographic data were refined in space group $P2_1/c$. The structure features a distorted octa-

Table 3. Selected Bond Lengths [Å] and Angles [deg] for Complexes **1a** and $\mathbf{3^{N3}}$[a]

1a		$\mathbf{3^{N3}}$	
Ru(1)−N(1)	2.064(6)	Ru(1)−N(1)	2.044(3)
Ru(1)−N(2)	2.072(6)	Ru(1)−N(2)	2.056(3)
Ru(1)−N(4)	2.062(6)	Ru(1)−N(3)	2.056(3)
Ru(1)−N(5)	2.070(6)	Ru(1)−N(4)	2.098(3)
Ru(1)−N(6)	2.085(6)	Ru(1)−N(6)	2.063(3)
Ru(1)−N(7)	2.066(6)	Ru(1)−N(7)	2.067(3)
C(4)−O(1)	1.27(1)	C(20)−O(1)	1.240(5)
C(4)−O(2)	1.28(1)	C(20)−O(2)	1.250(5)
N(1)−Ru(1)−N(2)	78.7(3)	N(1)−Ru1−N(2)	78.9(1)
N(1)−Ru(1)−N(4)	88.1(2)	N(1)−Ru1−N(3)	95.9(1)
N(1)−Ru(1)−N(5)	96.5(2)	N(1)−Ru1−N(4)	172.4(1)
N(1)−Ru(1)−N(6)	172.7(2)	N(1)−Ru(1)−N(6)	84.5(1)
N(1)−Ru(1)−N(7)	95.2(2)	N(1)−Ru(1)−N(7)	95.6(1)
N(2)−Ru(1)−N(4)	96.8(2)	N(2)−Ru(1)−N(3)	90.9(1)
N(2)−Ru(1)−N(5)	173.6(2)	N(2)−Ru(1)−N(4)	95.9(1)
N(2)−Ru(1)−N(6)	96.2(2)	N(2)−Ru(1)−N(6)	91.1(1)
N(2)−Ru(1)−N(7)	87.3(2)	N(2)−Ru(1)−N(7)	169.8(1)
N(4)−Ru(1)−N(5)	78.6(2)	N(3)−Ru(1)−N(4)	78.6(1)
N(4)−Ru(1)−N(6)	97.7(2)	N(3)−Ru(1)−N(6)	177.9(1)
N(4)−Ru(1)−N(7)	175.2(2)	N(3)−Ru(1)−N(7)	98.3(1)
N(5)−Ru(1)−N(6)	88.8(2)	N(4)−Ru(1)−N(6)	101.2(1)
N(5)−Ru(1)−N(7)	97.5(2)	N(4)−Ru(1)−N(7)	90.4(1)
N(6)−Ru(1)−N(7)	79.2(2)	N(6)−Ru(1)−N(7)	79.6(1)
		O(1)−C(20)−O(2)	127.3(4)

[a] esd in parenthesis.

Table 4. Summary of Visible Electronic Absorption Spectra of (10 ± 1) μM Acetonitrile Solutions of As-Dissolved, Fully Deprotonated and Fully Protonated **1**, **2**, and $\mathbf{3^{N3}}$

complex	λ_{max} (nm)	ε_{molar} (M^{-1} cm^{-1})	λ_{max} (nm)	ε_{molar} (M^{-1} cm^{-1})
1	422	10 100	450	11 400
1 + TEA	421	11 600	449	12 400
1 + TFA	428	13 700	475	11 100
2	419	11 300	447	12 100
2 + TEA	421	12 100	446	12 400
2 + TFA	429	13 800	475	10 600
$\mathbf{3^{N3}}$	432	10 000	454	11 800
$\mathbf{3^{N3}}$ + TEA			453	12 200
$\mathbf{3^{N3}}$ + TFA			439	11 000

hedral ruthenium(II) center coordinated to the N1 nitrogen atom of the protonated cppH ligand, two *cis*-carbonyl, and two *trans*-chloride ligands. The two Ru−N bond distances for the cppH ligand are similar (2.084(3) and 2.099(3) Å for Ru−N(1) and Ru(N(2), respectively). A slight distortion from octahedral geometry is reflected in trans C−Ru−N bond angles below 180° (174.1(1)° and 176.5(2)°) and *cis*−C−Ru−N angles below 90° (88.2(1)° and 87.1(1)°). The Ru−Cl and Ru−CO bond lengths of $[Ru^{II}(cppH)(CO)_2Cl_2]\cdot H_2O$ are in agreement with those observed for $[Ru^{II}(bpy)(CO)_2Cl_2]\cdot CH_2Cl_2$ (2.391(5)−2.390(5) Å and 1.899(11)−1.841(16) Å, respectively).[46] Figure 5B highlights the hydrogen bonding interactions in $[Ru^{II}(cppH)(CO)_2Cl_2]\cdot H_2O$. The water molecule is involved in hydrogen bonding to carboxylate groups from two different complexes and the chloride from a third complex. The coordination of the N1 nitrogen of cppH in this structure of indicates that **1** and **2** adopt the structures shown in Figure 1. The X-ray structure of **1a** supports this conclusion.

Crystals of **1a** and $\mathbf{3^{N3}}$ were found to be monoclinic and were refined in space groups *C*2/*c* and $P2_1/c$, respectively. A high degree of thermal motion in the PF_6^- anion and solvent water molecules led to a slightly higher *R* value than would be expected from R_{int}. The presence of one PF_6^- anion per ruthenium for **1a** and one NO_3^- anion per ruthenium for $\mathbf{3^{N3}}$ indicated that the complexes with the carboxylate groups deprotonated crystallized preferentially. The major difference in the two structures is that the carboxylate group in $\mathbf{3^{N3}}$ is oriented toward the ruthenium (II) center rather than away from it, as found for **1a** (see Figures 6 and 7A). This has arisen from the different synthetic protocol used to prepare the two complexes.

The geometry of the ruthenium(II) center in both **1a** and $\mathbf{3^{N3}}$ is distorted octahedral. The *trans*-N−Ru−N angles are below 180°, 172.7(2)° to 175.2(2)° for **1a** and 169.75(12)° to 177.91(12)° for $\mathbf{3^{N3}}$. The N−Ru−N "bite" angles for the bidentate ligands in **1a** (78.7(3)°, 78.6(2)°, and 79.2(2)°) and $\mathbf{3^{N3}}$ (78.56(13)°, 78.94(13)°, and 79.64(12)°) are typical of 5-membered chelate rings formed by such ligands and comparable to those in the related $[Ru(bpy)_2(4,4'\text{-}CO_2H\text{-}bpy)](PF_6)_2\cdot 3H_2O$ (78.5(3), 77.8(3), and 79.3(3)°). The Ru−N bond lengths found in **1a** (2.062(6)−2.085(6) Å) and $\mathbf{3^{N3}}$ (2.044(3)−2.056(3) Å) are in agreement with those for related structures.[26,47−49]

Another interesting feature in the structure of $\mathbf{3^{N3}}$ (shown in Figure 7B) is the presence of π-π bonding between adjacent cations forming a $(bipy\text{-}dppz\text{-}dppz\text{-}bipy)_n$ network. Each dppz ligand participates in π-π interactions with the dppz and bpy ligands of two different neighboring complex cations (plane to plane distance of 3.324 Å and 3.350 Å, respectively, defined as the distance between the centroid of C6, C7, C8, C9, C10, N2 and the dppz plane as the planes are not fully parallel)). These π-π interactions form a 3-dimensional infinite network linking up adjacent complex cations (Figure 7B). An interaction also exists between two adjacent ccp rings in $\mathbf{3^{N3}}$ (distance of 3.299 Å between the planes formed by the 12 atoms of the cpp ring). However, the overlap of the planes is not as significant as found in the $(bipy\text{-}dppz\text{-}dppz\text{-}bipy)_n$ network.

Electronic Spectroscopy and Electrochemistry

General Comments. As described in our earlier work,[26] small amounts of water in the isolated complexes or nonaqueous solvents used for the analysis can affect the degree of protonation of the carboxylate groups in complexes $\mathbf{1}-\mathbf{3^{N3}}$, as expressed in eq 1.

$$[Ru(L)(L')(cppH)]^{2+} \rightleftharpoons [Ru(L)(L')(cpp)]^{+} + H^{+} \quad (1)$$

where L = L′ or L ≠ L′. The study of the electronic spectroscopy and electrochemical oxidation of the cppH complexes includes an analysis of the acid and base dependence of these properties, gained through measurements on the as-dissolved, fully deprotonated and fully protonated species.

Electronic Absorption Spectra. The UV−visible spectra of complexes $\mathbf{1}-\mathbf{3^{N3}}$ were measured in acetonitrile at (10 ±

(46) Haukka, M.; Kiviaho, J.; Ahlgren, M.; Pakkanen, T., A. *Organometallics* **1995**, *14*, 825–833.

(47) Pearson, P.; Bond, A. M.; Deacon, G. B.; Forsyth, C.; Spiccia, L. *Inorg. Chim. Acta* **2007**, in press.

(48) Caspar, R.; Amouri, H.; Gruselle, M.; Cordier, C.; Malezieux, B.; Duval, R.; Leveque, H. *Eur. J. Inorg. Chem.* **2003**, *3*, 499–505.

Scheme 4. Protonation of **1′** in Excess TFA

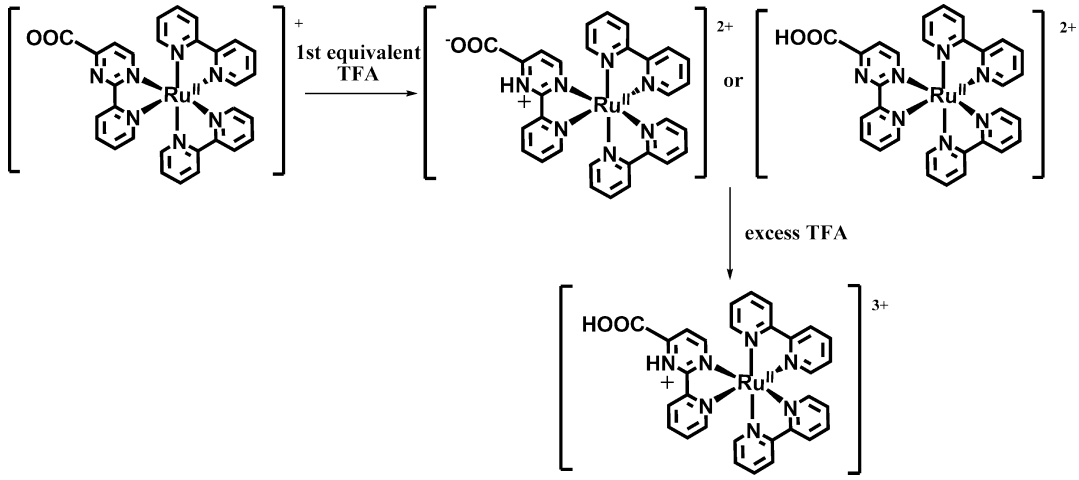

1) μM as follows: (a) as-dissolved; (b) with added triethylamine (TEA, 10-fold); and (c) with added trifluoroacetic acid (TFA, 10-fold) to obtain the spectra of the as-dissolved, predominantly depronated and protonated complexes, respectively. The spectral data are summarized in Table 4.

Consistent with the spectroscopic behavior of the prototype, $[Ru(bpy)_3]^{2+}$, the as-dissolved complexes exhibit intense bands at 450 nm, 447, and 455 nm, respectively, assigned to a MLCT (metal to ligand charge transfer, d→ π^*) transition. The shoulders observed at 422 and 419 nm in the spectra of **1** and **2**, respectively, are derived from the D_3 symmetry of the complex, which removes the degeneracy of the π^* levels.[13,28] Such a shoulder is not observable for $\mathbf{3^{N3}}$ and may be masked by overlapping MLCT bands. Two intense $\pi \rightarrow \pi^*$ intraligand transitions are found below 300 nm in the spectrum of **1** and **2** while for $\mathbf{3^{N3}}$ a characteristic $\pi \rightarrow \pi^*$ transition of the planar dppz ligand is observed at 355 nm.[50,51] In the presence of TEA, the absorption maxima of the MLCT bands for **1**, **2**, $\mathbf{3^{N3}}$ (449 nm, 446 nm, 456 nm, respectively) are similar to those observed for the as-dissolved forms, and slight decreases in the absorption intensities were observed as found for the [Ru(L)(L′)(Mebpy-COOH)]$^{2+}$ complexes (where L = L′ or L ≠ L′).[26,52] The assigned bands are also in agreement with studies involving the absorption of 2-(pyridyl)-2-pyridimidine attached ruthenium(II) complexes.[27,28] In the presence of excess TFA, the MLCT bands for **1** and **2** shift to 475 nm and broaden significantly. These shifts and appearance of much more intense shoulders at ~380nm were not observed on protonation of the Mebpy-COOH family of complexes but were in excellent agreement with observations made for the protonated $[Ru^{II}(bpy)_2(pypm)]^{2+}$ measured in aqueous solution.[29] The spectral changes may be rationalized in terms of changes in the energy levels of the ligand orbitals resulting from protonation of the uncoordinated nitrogen atom on the pyrimidine ring, as shown for complex **1** in Scheme 4. The similarity in the spectral changes for **1** and **2** indicate that they are associated with transitions from a metal orbital to an orbital on the protonated $cppH_2$ ligand. The main MLCT band of $\mathbf{3^{N3}}$ is largely unaffected by the addition of base. In contrast to **1** and **2**, however, addition of acid induced a blue shift in the emission maxima possibly indicating that the main transition involves electron transfer to the dppz ligand.

Table 5. Emission Spectral Data for $\mathbf{1}-\mathbf{3^{N3}}$ Measured in (10 ± 1) μM Acetonitrile Solutions on Excitation at 450 nm

complex	λ_{max} (nm)	I_s/I_{ref}	Φ_R[a]
1	622	0.84	0.044
1 + 10 equiv of TEA	623	1.23	0.070
1 + 10 equiv of TFA	669	0.50	0.028
2	618	1.41	0.073
2 + 10 equiv of TEA	617	1.18	0.064
2 + 10 equiv of TFA	654	0.94	0.052
$\mathbf{3^{N3}}$	663	0.28	0.016
$\mathbf{3^{N3}}$ + 10 equiv of TEA	626	0.09	0.005
$\mathbf{3^{N3}}$ + 10 equiv of TFA	671	0.11	0.006
$[Ru(bpy)_3]^{2+}$	615	1.00	0.062
$[Ru(bpy)_3]^{2+}$ + 10 equiv of TEA	615	1.03	0.059
$[Ru(bpy)_3]^{2+}$ + 10 equiv of TFA	615	1.10	0.064

[a] $\Phi_R = \Phi_{ref}(I_s A_{ref})/(I_{ref} A_s)$; where I_s and I_{ref} refer to the emission intensity calculated from the area under the emission spectrum of the sample and reference, respectively and A_s and A_{ref} refer to the absorbance of the sample and reference from the UV−vis spectra, respectively. $[Ru(bpy)_3]^{2+}$ was used as reference.

Emission Spectroscopy. A summary of emission spectral data for $\mathbf{1}-\mathbf{3^{N3}}$ measured at 273 K on excitation of (10 ± 1) μM acetonitrile solution at 450 nm are provided in Table 5. The emission wavelengths for the as dissolved complexes are in agreement with those observed for the corresponding complexes of MebpyCOOH.[13,26] On the basis of the assignment of the emission spectrum of the related $[Ru(bpy)_2(pym)]^{2+}$ (pym = 2-(pyridyl)-2-pyrimidine) and $[Ru(bpy)_3]^{2+}$, occurring via a high lying ^{3}MLCT excited state, the radiative decay of these complexes is also proposed to involve an ^{3}MLCT emission.[29] In the presence of TEA, the emission maxima of deprotonated **1** and **2** are similar to those obtained for the as-dissolved forms (c.f. 623 and 617 nm, respectively), suggesting that the complexes **1** and **2** are

(49) Caspar, R.; Musatkina, L.; Tatosyan, A.; Amouri, H.; Gruselle, M.; Cordier, C.; Guayard-Dhayon, C.; Duval, R. *Inorg. Chem.* **2004**, *43*, 7986–7993.
(50) Ambroise, A.; Maiya, B. G. *Inorg. Chem.* **2000**, *39*, 4256–4263.
(51) Fees, J.; Kaim, W.; Moscherosch, M.; Klima, J.; Krejcik, M.; Zalis, S. *Inorg. Chem.* **1993**, *32*, 166–174.
(52) Kilsa, K.; Mayo, E. I.; Brunschwig, B. S.; Gray, H. B.; Lewis, N. S.; Winkler, J. R. *J. Phys. Chem. B* **2004**, *108*, 15640–15651.

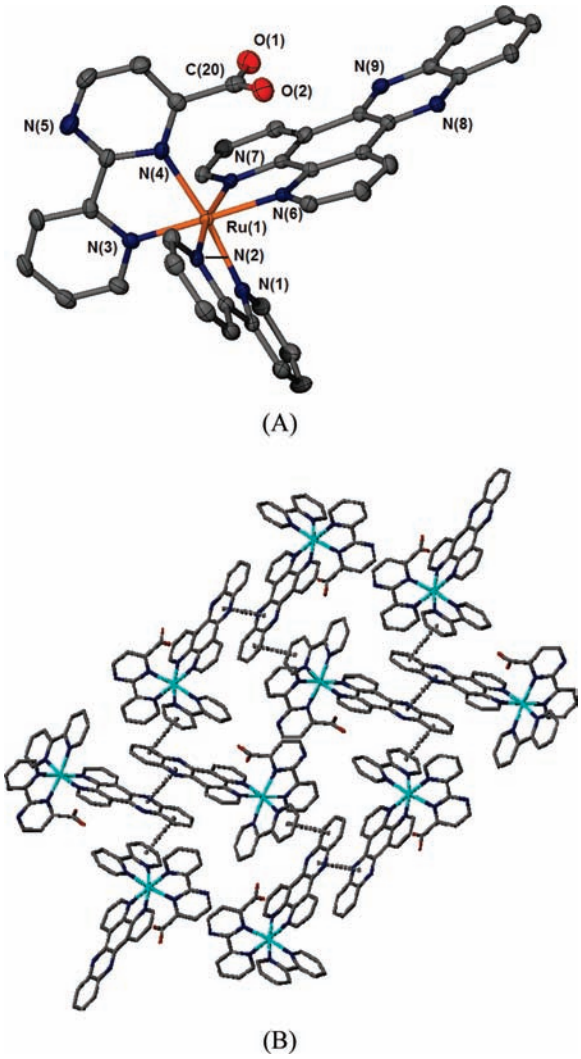

Figure 7. (A) Thermal ellipsoid representation of the cationic [Ru(bpy)-(cpp)(dppz)]$^{+}$ unit of $\mathbf{3^{N3}}$ (i) (probability ellipsoids drawn at 50%; hydrogen atoms and water molecules omitted for clarity and (B) $\pi\cdots\pi$ interactions of $\mathbf{3^{N3}}$, showing a 2-D infinite network. Scheme 4. Protonation of **1′** in excess TFA.

predominantly in their deprotonated form in solution. Compared to the as-dissolved complex, fully deprotonated $\mathbf{3^{N3}}$ exhibits a significant blue-shift in the emission maximum (626 nm) and a lowering in the emission intensity.

For bpy-carboxylate ligands coordinated to Ru^{II}, protonation of peripheral carboxylates typically results in red-shifts in the emission maxima coupled with significantly decreased emission intensities attributed to proton-induced quenching of the ^{3}MLCT excited-state and possible hydrogen-bonding.[26,53−55] The effect of protonation on the excited states of bipyrimidine and bipyrazine (bpz) attached ruthenium-(II) complexes have also been studied by Lever et al. [56] Protonation of non-coordinated nitrogen atoms on the diimine ligands coordinated to ruthenium(II) also leads to quenching of the ^{3}MLCT excited-state and subsequent weakened emission.[56,57] In agreement with these previous studies, the emission maxima of **1**, **2**, and $\mathbf{3^{N3}}$ are red-shifted on protonation and the intensities decrease (see Table 5).

Quantum yields were determined based on the work of Zhou et al. and our work[26,58] and are given in Table 5. The quantum yields of the as-dissolved and fully deprotonated **1** and **2** are similar and are consistent with those observed for the corresponding Mebpy-COO$^-$ analogues.[26] On addition of TFA, decreased emission intensities resulting from proton quenching lead to lower the quantum yields. The similar and low quantum yields observed for the deprotonated and fully protonated species $\mathbf{3^{N3}}$ complex are in keeping with previous observations for dppz bearing ruthenium(II) complexes in acetonitrile solutions.[59]

Electrochemistry. Cyclic Voltammetry. Cyclic voltammetry of $\mathbf{1-3^{N3}}$ at a stationary platinum (Pt) electrode was performed over the scan rate range of 10−1000 mV·s^{-1} in CH_3CN with tetrabutylammonium hexafluorophosphate (Bu_4NPF_6, 0.1 M) as the supporting electrolyte (Supporting Information, Table S1). Cyclic voltammograms at a scan rate of 50 mV s^{-1} are provided in Figure 8. Although ruthenium(II) complexes exhibit a series of ligand based reduction processes under voltammetric conditions, the present study reports only details of the oxidation of Ru^{II} to Ru^{III} as it is the key feature exploited in biosensing applications.

Reversible potentials (E^0_f values) were assumed to be equal to the midpoint potentials (E_m) and were determined from the average of the oxidation (E_p^{ox}) and reduction (E_p^{red}) peak potentials, $(E_p^{ox} + E_p^{red})/2$. Values for $\mathbf{1-3^{N3}}$ were 983 ± 3 mV, 1004 ± 5 mV, and 1023 ± 3 mV (vs Fc/Fc$^+$), respectively, for the Ru^{II}/Ru^{III} redox couple, as expressed in eq 2:

$$[Ru^{II}(L)(L')(cppH)]^{2+} \rightleftharpoons [Ru^{III}(L)(L')(cppH)]^{3+} + e^- \quad \text{where} \quad L = L' \text{ or } L \neq L' \quad (2)$$

Differences between peak oxidation and reduction potentials are close to that observed for the reversible $Fc^{0/+}$ couple (76 mV) measured at 100 mV s^{-1}, indicating that these processes are electrochemically reversible and monoelectronic. Plots of the oxidation peak current, I_p^{ox}, versus the square root of scan rate were linear in each case, confirming that the Ru^{II}/Ru^{III} process was mass transport controlled. The values of $|I_p^{ox}/I_p^{red}|$ are close to unity (see Supporting Information, Table S1) as expected for a chemically reversible system.

E^0_f values obtained for the Ru^{II}/Ru^{III} couple for $\mathbf{1-3^{N3}}$ are more positive than $[Ru(bpy)_3]^{2+}$ (+ 888 mV vs $Fc^{0/+}$) but similar to ruthenium(II) complexes with attached carboxylic acid moieties.[26,47] Unlike for some other systems, evidence for a pre-wave corresponding to kinetically controlled oxidation of the deprotonated complex was minimal for **1**

(53) Giordano, P. J.; Bock, C. R.; Wrighton, M. S.; Interrante, L. V.; Williams, R. F. X. *J. Am. Chem. Soc.* **1977**, *99*, 3187–3189.
(54) Zheng, G. Y.; Wang, Y.; Rillema, D. P. *Inorg. Chem.* **1996**, *35*, 7118–7123.
(55) Cherry, W. R.; Henderson, L. J. *Inorg. Chem.* **1984**, *23*, 983–986.
(56) Crutchley, R. J.; Kress, N.; Lever, A. B. P. *J. Am. Chem. Soc.* **1983**, *105*, 1170.
(57) Rillema, D. P.; Allen, G.; Meyer, T. J.; Conrad, D. *Inorg. Chem.* **1983**, *22*, 1617–1622.
(58) Zhou, M.; Robertson, G. P.; Roovers, J. *Inorg. Chem.* **2005**, *44*, 8317–8325.
(59) Metcalfe, C.; Thomas, J. A. *Chem. Soc. Rev.* **2003**, *32*, 215–224.

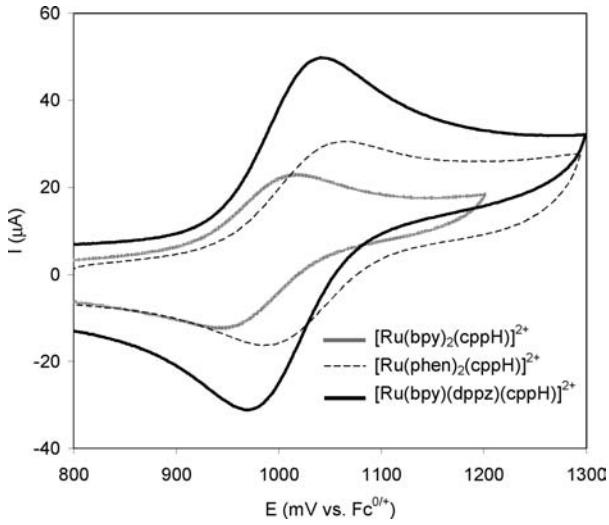

Figure 8. Cyclic voltammograms obtained at a Pt working electrode (0.0079 cm^2) using a scan rate of 50 mV s^{-1} for oxidation of **1** (0.77 mM), **2** (1.02 mM), and $\mathbf{3^{N3}}$ (0.89 mM) in MeCN (0.1 M $^nBu_4NPF_6$).

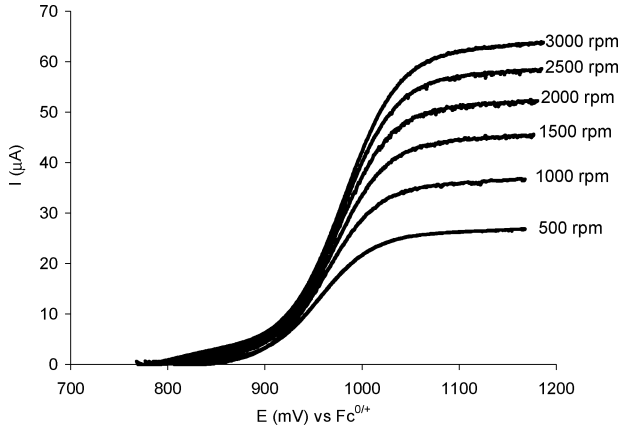

Figure 9. Platinum rotated disk electrode (0.071 cm^2) voltammograms obtained for 0.77 mM fully dissolved **1** in MeCN (0.1 M $^nBu_4NPF_6$) using a range of rotation rates from 500 to 3000 rpm at a scan rate of 10 mV s^{-1}.

and $\mathbf{3^{N3}}$ and not detected for **2**. Addition of TFA produced ideal single reversible oxidation processes at the same potentials as in the absence of acid.

The reversible potentials can be systematically varied through ligand substitution as seen with the series of cppH attached Ru^{II} complexes. Increased electron delocalization in going from complex **1** to $\mathbf{3^{N3}}$ gives rise to more positive $E°_f$ values as reflected in eq 3.

$$E°_f[Ru(bpy)_2(cppH)]^{2+} < [Ru(phen)_2(cppH)]^{2+} < [Ru(bpy)(dppz)(cppH)]^{2+} \quad (3)$$

Rotated Disc Electrode Voltammetry. Rotated disk electrode voltammetry of $\mathbf{1-3^{N3}}$ was investigated at rotation rates over the range of 500 to 3000 rpm with a scan rate of 10 mV s^{-1}. Voltammograms for **1** are shown in Figure 9 while those for **2** and $\mathbf{3^{N3}}$ are provided as Supporting Information. Half-wave potentials denoted as $E_{1/2}$ values (potential where the current is half the value ($I_L/2$) of the limiting current, I_L) for $\mathbf{1-3^{N3}}$ were observed at 985 ± 5 mV, 1007 ± 5 mV, and 1034 ± 5 mV versus $Fc^{0/+}$, respectively. Further details of rotating disk voltammetric data are available in Table S1. As expected for a reversible process, rotated disk electrode voltammograms for $\mathbf{1-3^{N3}}$ exhibited sigmoidal shaped curves with $E_{1/2}$ values being close to $E°_f$ values obtained from cyclic voltammetry. Consistent with the cyclic voltammetry, the limiting currents found for $\mathbf{1-3^{N3}}$ are linearly dependent on the square root of the rotation rate, as expected for processes that are mass transport controlled. The diffusion coefficients were determined through the use of Levich equation[60] expressed in eq 4

$$i_L = 0.620nFAD^{2/3}\omega^{1/2}\upsilon^{-1/6}C_0 \quad (4)$$

where n is the number of electrons transferred ($n = 1$), F is Faraday's constant, A is the electrode area (cm^2), ω is the angular velocity of the electrode (s^{-1}), υ is the kinematic viscosity of the solvent ($\upsilon_{MeCN} = 0.0045$ cm^2 s^{-1}), C_0 is the bulk concentration (mol cm^{-3}), and D is the diffusion coefficient (cm^2 s^{-1}).

The diffusion coefficient values of **1** (9.9 ± 0.1) × 10^{-6} cm^2 s^{-1}, **2** (1.1 ± 0.1) × 10^{-5} cm^2 s^{-1}, and $\mathbf{3^{N3}}$ (9.6 ± 0.1) × 10^{-6} cm^2 s^{-1} are close to the reported diffusion coefficient value of 9.7 × 10^{-6} cm^2 s^{-1} for $Ru(bpy)_3^{2+}$ in MeCN and those of Mebpy-COOH bearing Ru^{II} complexes.[61] As under conditions of cyclic voltammetry, a small contribution of a pre-wave attributed to kinetically controlled oxidation of the deprotonated form is found for **1** and $\mathbf{3^{N3}}$ but not **2**. The pre-wave is absent after addition of acid.

Spectroelectrochemistry. The voltammetry data imply the existence of stable Ru^{III} complexes. To further probe the metal based (Ru^{II}/Ru^{III}) redox process, Optically Transparent Thin-Layer Electrolysis (OTTLE) experiments were conducted. In the case of $Ru^{II}(bpy)_2(cppH)]^{2+}$, a constant potential of 1250 mV (vs Fc/Fc^+) was applied at a platinum gauze electrode to a 0.13 mM acetonitrile solution, and the oxidation to Ru^{III} in situ was monitored by UV−visible spectrophotometry (Figure 10a). The disappearance of the band at 285 nm in the UV region of the spectrum was accompanied by the growth of two overlapping bands at 305 nm and ~313 nm, while the band at 246 nm increased in intensity. In the visible region, the band in the 450 nm region decreased in intensity, and the oxidized species displayed only one very weak band at 420 nm. Isosbestic points were observed at 330, 297, and 265 nm. After 10 min of electrolysis, the spectral changes were complete. After the potential was removed, no reconversion to $Ru^{II}(bpy)_2$-$(cppH)]^{2+}$ occurred. Thus, despite the low concentration used and the very positive potential (thermodynamically making the compound capable of oxidizing trace amounts of adventitious water), no evidence for any instability was detected. However, on altering the potential to 700 mV versus $Fc^{0/+}$, complete reversion to $Ru^{II}(bpy)_2(cppH)]^{2+}$ was achieved. All

(60) Levich, V. G., *Physicochemical Hydrodynamics*; Prentice-Hall, Englewood Cliffs: New Jersey, 1962.
(61) McDevitt, M. R.; Addison, A. W. *Inorg. Chim. Acta* **1993**, *204*, 141–146.
(62) Bryant, G. M.; Fergusson, J. E. *Aust. J. Chem.* **1971**, *24*, 275.
(63) Nazeeruddin, M. K.; Zakeeruddin, S. M.; Kalyanasundaram, K. *J. Phys. Chem.* **1993**, *97*, 9607–9612.

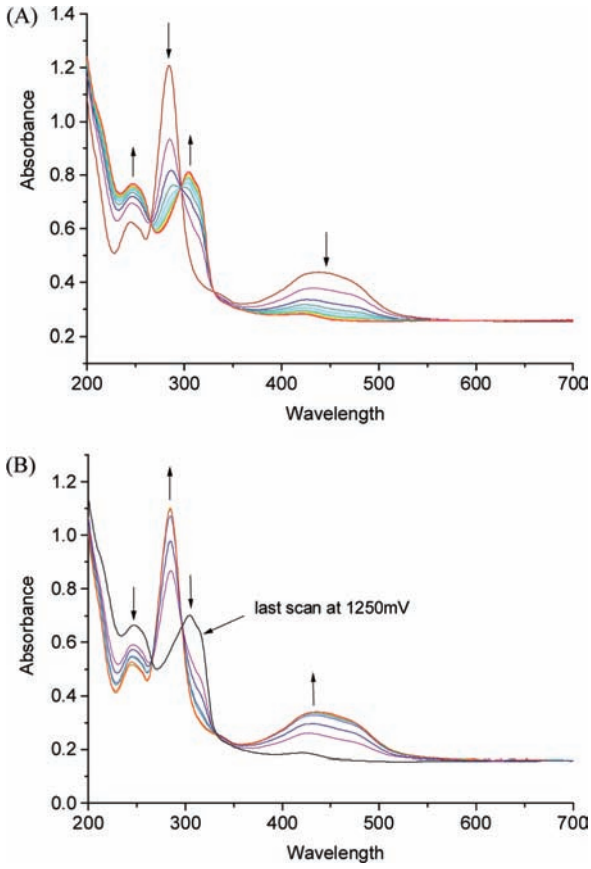

Figure 10. OTTLE experiments for the (a) oxidation of $[Ru^{II}(bpy)_2(cppH)]^{2+}$ (0.13 mM in MeCN (0.1 M $^nBu_4NPF_6$), $E_{applied} = 1250$ mV vs $Fc^{0/+}$, Pt electrode) and (b) reduction of $[Ru^{III}(bpy)_2(cppH)]^{2+}$ (0.13 mM in MeCN (0.1 M $^nBu_4NPF_6$), $E_{applied} = 700$ mV vs $Fc^{0/+}$, Pt electrode).

these data are consistent with the chemically reversible process

$$Ru^{II}(bpy)_2(cppH)]^{2+} \rightleftharpoons Ru^{III}(bpy)_2(cppH)]^{3+} + e^- \quad (5)$$

The three bands in the ultraviolet region observed for the electro-generated Ru^{III} complex at 246 nm and two overlapping bands at 305/313 nm have been assigned to intraligand ($\pi \rightarrow \pi^*$) transitions of the bipyridyl ligand.[62,63] The weak band observed in the visible region at 420 nm is attributable to a LMCT transitions ($\pi \rightarrow t_2$).[62] Comparison of Figure 10a and 10b shows that after the electrolysis at reductive potential (700 mV vs $Fc^{0/+}$) the spectrum resembles that of the initial complex, $[Ru^{II}(bpy)_2(cppH)]^{2+}$.

Conclusions

A new bidentate ligand, 2-(2′-pyridyl)pyrimidine-4-carboxylic acid (cppH), has been developed and applied in the synthesis of a series of ruthenium(II) complexes of cppH, $[Ru(bpy)_2(cppH)](PF_6)_2 \cdot H_2O$ (**1**), $[Ru(phen)_2(bpy\text{-}COOH)](PF_6)_2$ (**2**), and $[Ru(bpy)(dppz)(cppH)](PF_6)_2$ (**3**), via an established decarbonylation methodology. The X-ray structure of **1a**, a deprotonated derivative of **1**, revealed that the isomer formed was that expected on the basis of the structure of the precursor to **1**, $[Ru^{II}(cppH)(CO)_2Cl_2] \cdot H_2O$. That is, the pyrimidine nitrogen para rather than that ortho to the carboxylate group coordinates to ruthenium(II). In contrast, the synthesis of **3** leads to a mixture of isomers from which $\mathbf{3^{N3}}$ was isolated as the major product. An X-ray structure determination on this complex unexpectedly found that the pyrimidine nitrogen ortho to the carboxylate is coordinated and that the deprotonated carboxylate group is oriented toward rather that away from the ruthenium(II) center, as found for **1** and $[Ru^{II}(cppH)(CO)_2Cl_2] \cdot H_2O$. The major difference in synthetic procedure was that cppH was added in the final decarbonylation step rather than first, as was the case for **1** and **2**. Under these conditions, ligand addition appears to be less controlled leading to a mixture of products, of which $\mathbf{3^{N3}}$ crystallizes most easily. The complexes exhibited changes in UV−visible and emission spectra that were in keeping with previous studies on a series of Mebpy-COOH analogues. Electrochemical studies of $\mathbf{1}-\mathbf{3^{N3}}$ showed reversible Ru^{II}/Ru^{III} oxidation process at E^0_f values of 987 mV, 1004 mV, and 1023 mV (vs Fc/Fc^+). The order of redox potentials, $\mathbf{1} < \mathbf{2} < \mathbf{3}$, indicated an increase in stability of the ruthenium(II) state which mirrors the increased aromaticity of the ligands. Future research will aim to explore the use of these promising complexes in biosensing applications.

Acknowledgment. We acknowledge financial support of this work by the Australian Research Council through the Australian Centre for Electromaterials Science (ACES) and the Federation Fellowship Scheme (A.M.B.). N.N. is the recipient of a Monash Departmental Scholarship.

Supporting Information Available: X-ray crystallographic files for 1a and 2a in CIF format; representative examples of the ^1H NMR of mpp, cppH and complexes $\mathbf{1}-\mathbf{3^{N3}}$ (Figures S1−S6); electronic spectra (Figure S7); emission spectra (Figures S8−S10); cyclic voltammograms of $\mathbf{1}-\mathbf{3^{N3}}$as a function of scan rate (Figures S11−13); rotated disk voltammograms (Figures S14 and S15) and voltammetric data **1**, **2**, and $\mathbf{3^{N3}}$ (Table S1). This material is available free of charge via the Internet at http://pubs.acs.org.

IC800972X